

NO-A187 578

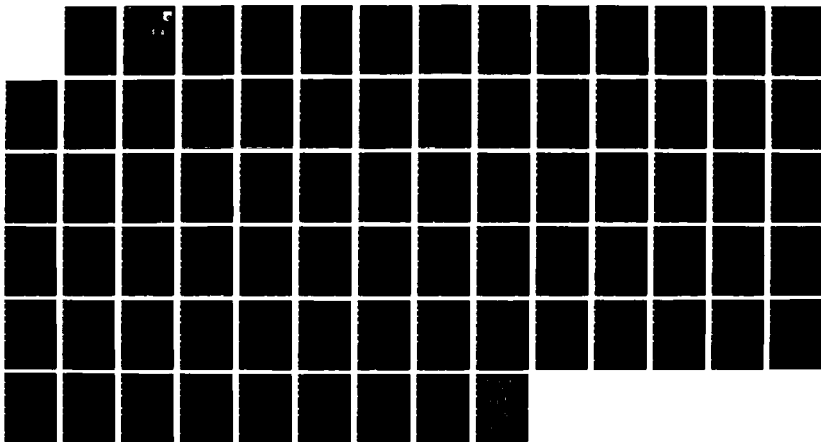
BACKSCATTERING FROM THREE DIMENSIONAL CONDUCTING BODIES 1/1
(U) CALIFORNIA UNIV LOS ANGELES DEPT OF ENGINEERING
SYSTEMS C T LEONDES OCT 87 AFWAL-TR-87-1134

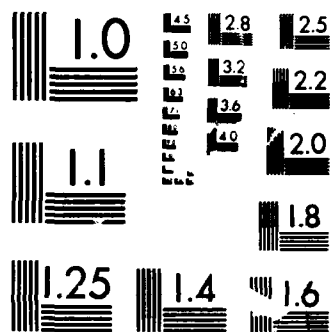
UNCLASSIFIED

F33615-77-C-1281

F/G 17/9

NL





MICROCOPY RESOLUTION TEST CHART
NATIONAL BUREAU OF STANDARDS-1963-A

DTIC FILE COPY

AD-A187 570

AFWAL-TR-87-1134

BACKSCATTERING FROM THREE D MENSIONAL CONDUCTING BODIES



Dr. Cornelius T. Leondes
University of California
Department of Engineering Systems
Los Angeles CA 90024

DTIC
ELECTE
NOV 10 1987
S D

October 1987

Final Report for Period Aug 77 - Sept 78

Approved for public release; distribution unlimited.

AVIONICS LABORATORY
AIR FORCE WRIGHT AERONAUTICAL LABORATORIES
AIR FORCE SYSTEMS COMMAND
WRIGHT-PATTERSON AIR FORCE BASE, OHIO 45433-6543

NOTICE

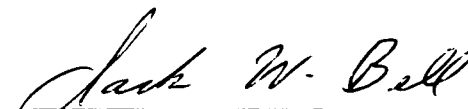
When Government drawings, specifications, or other data are used for any purpose other than in connection with a definitely related Government procurement operation, the United States Government thereby incurs no responsibility nor any obligation whatsoever; and the fact that the government may have formulated, furnished, or in any way supplied the said drawings, specifications, or other data, is not to be regarded by implication or otherwise as in any manner licensing the holder or any other person or corporation, or conveying any rights or permission to manufacture use, or sell any patented invention that may in any way be related thereto.

This report has been reviewed by the Office of Public Affairs (ASD/PA) and is releasable to the National Technical Information Service (NTIS). At NTIS, it will be available to the general public, including foreign nations.

This technical report has been reviewed and is approved for publication.

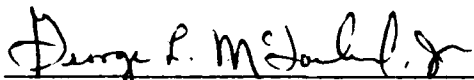


HAROLD W. NOFFKE
Project Engineer
Analysis And Signal
Processing Group



DR JACKIE W. BELL
Chief, Analysis And Signal
Processing Group
Radar Branch

FOR THE COMMANDER



GEORGE L. McFARLAND, JR.
Chief, Radar Branch
Mission Avionics Division
Avionics Laboratory

If your address has changed, if you wish to be removed from our mailing list, or if the addressee is no longer employed by your organization please notify AFWAL/AARM, W-PAFB, OH 45433 to help us maintain a current mailing list.

Copies of this report should not be returned unless return is required by security considerations, contractual obligations, or notice on a specific document.

REPORT DOCUMENTATION PAGE

1a. REPORT SECURITY CLASSIFICATION UNCLASSIFIED			1b. RESTRICTIVE MARKINGS None		
2a. SECURITY CLASSIFICATION AUTHORITY			3. DISTRIBUTION/AVAILABILITY OF REPORT Approved for public release; distribution unlimited.		
2b. DECLASSIFICATION/DOWNGRADING SCHEDULE					
4. PERFORMING ORGANIZATION REPORT NUMBER(S)			5. MONITORING ORGANIZATION REPORT NUMBER(S) AFWAL-TR-87-1134		
6a. NAME OF PERFORMING ORGANIZATION University of California Los Angeles (UCLA)		5b. OFFICE SYMBOL (If applicable)	7a. NAME OF MONITORING ORGANIZATION Avionics Laboratory (AFWAL/AARM) AF Wright Aeronautical Laboratories		
6c. ADDRESS (City, State and ZIP Code) Department of Engineering Systems University of California At Los Angeles Los Angeles CA 90024			7b. ADDRESS (City, State and ZIP Code) WPAFB OH 45433-6543		
8a. NAME OF FUNDING/SPONSORING ORGANIZATION Avionics Laboratory		8b. OFFICE SYMBOL (If applicable) AFWAL/AARM-3	9. PROCUREMENT INSTRUMENT IDENTIFICATION NUMBER Contract No. F33615-77-C-1201		
8c. ADDRESS (City, State and ZIP Code) AFWAL/AARM-3 WPAFB OH 45433-6543			10. SOURCE OF FUNDING NOS.		
			PROGRAM ELEMENT NO. 62204F	PROJECT NO. 7622	TASK NO. 01
			WORK UNIT NO. 43		
11. TITLE (Include Security Classification) Backscattering From Three Dimensional Bodies					
12. PERSONAL AUTHOR(S) Dr Cornelius T. Leondes					
13a. TYPE OF REPORT Final		13b. TIME COVERED FROM 770801 TO 780930		14. DATE OF REPORT (Yr., Mo., Day) 1987 October	
				15. PAGE COUNT 73	
16. SUPPLEMENTARY NOTATION					
17. COSATI CODES			18. SUBJECT TERMS (Continue on reverse if necessary and identify by block number)		
FIELD	GROUP	SUB. GR.			
09	03		Backscattering, Geometric Theory of Diffraction,		
09	02		Synthetic Aperture Radar		
19. ABSTRACT (Continue on reverse if necessary and identify by block number)					
<p>The report investigates electromagnetic backscattering from three dimensional objects. It uses the following simulation approaches: physical optics together with the physical theory of diffraction; numerical methods; geometrical optics with the geometric theory of diffraction. Physical objects modelled are a sphere and a spherical segment.</p> <p>The report concludes that geometrical optics together with the geometric theory of diffraction is the most practical way of calculating EM backscatter from conducting objects.</p> <p><i>... for radar target modeling</i></p>					
20. DISTRIBUTION/AVAILABILITY OF ABSTRACT UNCLASSIFIED/UNLIMITED <input checked="" type="checkbox"/> SAME AS RPT <input type="checkbox"/> DTIC USERS <input type="checkbox"/>			21. ABSTRACT SECURITY CLASSIFICATION UNCLASSIFIED		
22a. NAME OF RESPONSIBLE INDIVIDUAL HAROLD W. NOFFKE			22b. TELEPHONE NUMBER (Include Area Code) 513-255-3655		22c. OFFICE SYMBOL AFWAL/AARM-3

SECURITY CLASSIFICATION OF THIS PAGE

SECURITY CLASSIFICATION OF THIS PAGE

ACKNOWLEDGEMENTS

Our heartfelt thanks are due to Dr. Cornelius T. Leondes for his constant encouragement all along the various stages of the report. We wish to thank Mr. Harold Noffke of the Air Force Avionics Laboratory at Wright Patterson Air Force Base for his help in the administrative details of the research involved. Our special thanks are due to Mrs. Frances Lynch who has always been friendly and ready to help, and who typed this report meticulously.

We sincerely thank the United States Air Force Avionics Laboratory for their financial support without which this report would not have been completed.

Arunkumar P. Nayak, Research Engineer

Hagop Panossian, Research Engineer

Accession For	
NTIS CRA&I	<input checked="checked" type="checkbox"/>
DTIC TAB	<input type="checkbox"/>
Unannounced	<input type="checkbox"/>
Justification	
By	
Distribution/	
Availability Codes	
Dist	Availability for Special
A-1	

TABLE OF CONTENTS

	page
FIGURES	v
CHAPTER 1 - INTRODUCTION	1
CHAPTER 2 - THEORY OF SCATTERING	3
2.1 Wave Propagation	4
2.2 Boundary and Radiation Condition	4
2.3 Integral Equations	5
2.4 Physical Optics	6
2.5 Physical Theory of Diffraction	8
2.6 Numerical Methods	10
2.7 Geometrical Optics	11
2.8 Geometrical Theory of Diffraction	12
CHAPTER 3 - THE CHOICE OF METHOD	28
CHAPTER 4 - APPLICATIONS	30
4.1 Backscattering from a Sphere	30
4.2 Backscattering from a Spherical Segment	33
CHAPTER 5 - HIERARCHY PLUS INPUT-PROCESS-OUTPUT CHARTS	48

TABLE OF CONTENTS (continued)

CHAPTER 6 - DISCUSSION AND SUGGESTIONS 43

REFERENCES 51

APPENDIX I 53

FIGURES

Number		page
1	General Coordinates of the Problem	7
2	Scattering by Geometrical Optics	15
3	Edge Diffraction	19
4	Edge Diffraction, General Picture	19
5	Edge Fixed Plane of Incidence and Diffraction . . .	22
6	Curved Edge Diffraction	22
7	Surface Diffraction (Top View)	27
8	Surface Diffraction (Side View)	27
9	Backscatter from a Sphere	32
10	Backscatter from a Spherical Segment, a General Picture	35
11	Backscattering from One Point	37
12	Backscattering from Two Points	37
13	Backscattering from Three Points	37
14	Backscattering from a Spherical Segment (Top View)	40
15	Backscattering from a Spherical Segment, the Coordinate Plane	40
16	Backscattering from a Spherical Segment, the Skew View	40

ABSTRACT OF REPORT

Backscattering from Three
Dimensional Conducting Bodies

by

Arunkumar P. Nayak
and

Hagop Panossian

University of California, Los Angeles
School of Engineering and Applied Science

Principal Investigator
Professor Cornelius T. Leondes

It is our endeavor here to develop a more reliable and complete Synthetic Aperture Radar target modeling capability. The algorithm to solve such problems should be practically feasible and accurate. It must also have wide range of application.

The main core of the study is to calculate the electromagnetic (EM) backscattering from life-size objects like a car or a tank, etc. To accomplish that, we will pursue high frequency methods.

The three most popular high frequency methods are discussed. They are (i) Physical Optics together with Physical Theory of

Diffraction, (ii) Numerical methods, and (iii) Geometrical Optics in conjunction with Geometrical Theory of Diffraction. We found that Geometrical Optics together with Geometrical Theory of Diffraction is the most practical way of calculating EM Backscatter from conducting objects. Also, it is easier to apply and has conceptual simplicity.

After making the choice of the method, we applied them to calculate EM backscatter from a sphere and a spherical segment. The latter object is a simplified model of a car.

We have given all the equations in detail for three cases and also we have given Hierarchical plus Input-Process-Output charts for the case of overview and coding purposes.

CHAPTER ONE

INTRODUCTION

It is our endeavor here to develop a more reliable and complete Synthetic Aperture Radar target modeling capability. The algorithm to solve such problems should be practically feasible and accurate. It must also have wide range of application.

The main objective of the study is to calculate the electromagnetic (EM) scattering from life size objects like a car or a tank, etc. To accomplish that we will pursue high frequency techniques. When the wavelength is small compared to the characteristic dimensions of the scattering body, which is so in our case, asymptotic high frequency methods must be used.

We begin with the basics of the electromagnetics, namely the Maxwell's equations and move on to the discussion of the three most popular high frequency methods. These three methods are (i) Physical Optics together with Physical Theory of Diffraction, (ii) Numerical Methods, (iii) Geometrical Optics in conjunction with Geometrical Theory of Diffraction. After doing some deep probing we have come to a conclusion that Geometrical Optics combined with Geometrical Theory of Diffraction is the most practical method for calculating EM scattering from objects. The method is general enough to consider any kind of polarization.

After making a choice of the method we applied it to calculate the EM backscattering from a sphere and a spherical segment. The latter object is a simplified model of a car.

The method has been documented in order to facilitate an overview of the system and to determine program functions for coding purposes. The method used to document is called Hierarchy plus Input-Process-Output (HIPO) which is developed by IBM.

CHAPTER TWO

THEORY OF SCATTERING

The electromagnetic field at a time t and at any point in a linear, homogeneous and isotropic medium of electric permittivity ϵ , magnetic permeability μ , and zero conductivity is described by the homogeneous Maxwell's equations

$$\nabla \times \vec{H} = \epsilon \frac{\partial \vec{E}}{\partial t} \quad (1)$$

$$\nabla \times \vec{E} = -\mu \frac{\partial \vec{H}}{\partial t} \quad (2)$$

and auxiliary equation

$$\nabla \cdot \vec{H} = \nabla \cdot \vec{E} = 0 \quad (3)$$

which govern the behavior of the electric field \vec{E} and of the magnetic field \vec{H} at all ordinary points in the space.

In the following we shall consider only the particular case of monochromatic radiation.

If a scattering body is embedded in the medium, (1), (2), and (3) are satisfied by the incident or primary fields \vec{E}^i and \vec{H}^i , by the total (incident plus scattered) fields \vec{E} and \vec{H} and therefore also by the secondary or scattered fields \vec{E}^s and \vec{H}^s , which represent the disturbance added to the primary fields by the scatterer.

The wave number k and the intrinsic impedance Z of the medium surrounding the scatterer are given by

$$k = \omega \sqrt{\epsilon\mu} = 2\pi/\lambda \quad (4)$$

$$Z = Y^{-1} = \sqrt{\mu/\epsilon} \quad (5)$$

where ω is the angular frequency and λ the wavelength. The time dependence factor $\exp(-j\omega t)$ is suppressed throughout. So the Eq. (1) and (2) will become

$$\nabla \times \vec{H} = -jkY\vec{E} \quad (6)$$

$$\nabla \times \vec{E} = jkZ\vec{H} \quad (7)$$

2.1 Wave Propagation

For harmonic time dependence it can be shown from Eq. (1), (2), and (3) that

$$(\nabla^2 + k^2)\vec{H} = 0 \quad (8)$$

$$(\nabla^2 + k^2)\vec{E} = 0 \quad (9)$$

with the auxiliary condition

$$\nabla \cdot \vec{H} = \nabla \cdot \vec{E} = 0 \quad (3)$$

2.2 Boundary and Radiation Condition

We are going to limit our considerations to perfect conductors, i.e., we require that the tangential component of the total electric field at any regular point of the scattering surface be zero.

$$\vec{E} - (\vec{E} \cdot \hat{n})\hat{n} = 0 \quad (10)$$

where \hat{n} is the unit normal to the surface directed from the body into the surrounding medium. It is seen from Maxwell's equations that

condition (10) implies that the normal component of the total magnetic field is zero at any regular point of the surface scatterer.

2.3 Integral Equations

For an electromagnetic wave incident on a body, integral equations can be derived from which to determine the fields induced on the surface of the scatterer.

It is convenient to confine attention to a three-dimensional, closed and bounded body whose surface S is regular.

Stratton [1] has given the necessary equation

$$\vec{E}(\mathbf{r}) = \vec{E}^1(\mathbf{r}) + \int_S \{jkZ(\hat{n}_1 \times \vec{H})\psi + (\hat{n}_1 \times \vec{E}) \times \nabla\psi + (\hat{n}_1 \cdot \vec{E})\nabla\psi\} ds \quad (11)$$

$$\vec{H}(\mathbf{r}) = \vec{H}^1(\mathbf{r}) - \frac{1}{4\pi} \int_S \{jkY(\hat{n}_1 \times \vec{E})\psi - (\hat{n}_1 \times \vec{H}) \times \nabla\psi - (\hat{n}_1 \cdot \vec{H})\nabla\psi\} ds \quad (12)$$

Maue [2] has given an expression for surface current which follows from Eq. (12)

$$2\hat{n}(\mathbf{r}) \times \vec{H}^1(\mathbf{r}) = \vec{J}(\mathbf{r}) - \frac{1}{2\pi} \hat{n}(\mathbf{r}) \times \int_S \vec{J}(\mathbf{r}_1) \times \nabla\psi ds_1 \quad (12a)$$

$$\psi = \exp(jkR)/R \quad (13)$$

$$R = |\vec{r} - \vec{r}_1| \quad (14)$$

$$\mathbf{r}, \mathbf{r}_1 \in S$$

The del operator operates on the surface pt. \mathbf{r}_1 only.

If the body is perfectly conducting, the surface current density

$$\vec{J} = 2\hat{n} \times \vec{H}^i \quad (15)$$

and this follows immediately from Eq. (12a).

2.4 Physical Optics (PO)

"Physical Optics" denotes an approximate method for the determination of the field scattered by an object through an assumption about the specific form of the field distribution on the surface. Explicitly, it is assumed that the field there is the geometrical optics surface field, implying that at each point on the geometrically illuminated side of the body the scattering at the surface takes place as though from an infinite tangent plane at the point, whereas over the shadowed portion of the body the surface field is zero. For a perfectly conducting body the postulated current distribution is therefore

$$\begin{aligned} \vec{J} &= 2\hat{n} \times \vec{H}^i \quad \text{on the illuminated side} \\ &= 0 \quad \text{on the shadowed side.} \end{aligned} \quad (15)$$

where \hat{n} is a unit vector normal drawn outwards as regards body. \vec{H}^i is the incident magnetic field. The scattered fields radiated by these currents are given by Rusch and Potter [3].

$$\vec{E}(p) = - \frac{j\omega\mu}{4\pi} \int_S \left\{ \vec{J}\psi + \frac{1}{k^2} (\vec{J} \cdot \nabla) \nabla\psi \right\} ds \quad (16)$$

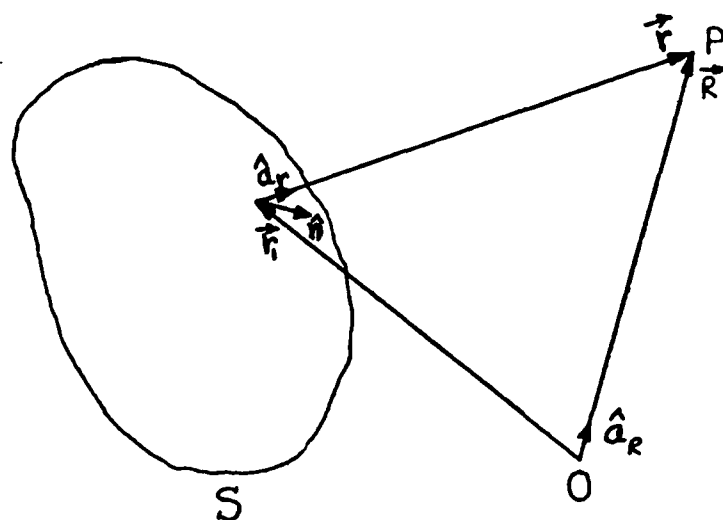


Fig. 1

$$\vec{H}(p) = \frac{1}{4\pi} \int_S [\vec{J} \times \nabla \psi] ds \quad (17)$$

when $r \gg \lambda$ we can approximate

$$\vec{E}^s(p) = -\frac{j\omega\mu}{4\pi} \psi \int_S [\vec{J} - (\vec{J} \cdot \hat{a}_R) \hat{a}_R] \exp(jk\vec{r}_1 \cdot \hat{a}_R) ds \quad (18)$$

$$\vec{H}^s(p) = \frac{jk}{4\pi} \psi \int_S [\vec{J} \times \hat{a}_R] \exp(jk\vec{r} \cdot \hat{a}_R) ds \quad (19)$$

$$\psi = \exp(-jkR)/R, \quad R = |\vec{R}| \quad (20)$$

In contrast to the geometrical optics expression for the scattered field, the above integrals are frequency dependent, and it is therefore possible that physical optics provides a more accurate estimate of the scattering.

Physical optics provide an accurate estimate of scattering whenever this arises from a portion of the surface where the actual surface field is adequately approximated by the postulated distribution. If a body has one (or both) of its radii of curvature infinite at the specular point, the geometrical optics cross section is infinite, and a particular advantage of the physical optics is that a bounded (and wavelength dependent) estimate of the scattering cross section can be now estimated.

2.5 Physical Theory of Diffraction (PTD)

PTD is an integrative technique in which the surface field of Geometrical Optics (GO) is refined by the addition of a nonuniform edge component. The method is therefore an extension of Physical Optics (PO)

and since the nonuniform component is, in principle, approximated in terms of the surface field on a (local) wedge, the result should constitute a caustically corrected version of the GTD prediction. A description of the method is given in Ufimtsev's monograph [4].

Ufimtsev postulates that the total induced surface current J can be represented as the sum of two components, one the physical optics current J_0 , and the other J_1 , a correction to J_0 due to all other effects not included in PO.

$$J = J_0 + J_1 \quad (21)$$

Ufimtsev refers to these two currents as the "uniform" and "nonuniform" components, respectively. J_0 is the GO field on an infinite flat surface tangent to the body at the point in question. The J_1 is due to perturbations created by the departure of the surface from an infinite plane. In his monograph [4] and other publications, Ufimtsev considers only the nonuniform component due to edges and in practice, therefore, PTD is a high frequency method for estimating scattering by edged bodies.

The nonuniform component near an edge is approximated by the current appropriate to an infinite wedge, or half-plane tangent to the edge and the fields scattered by an edged structure are then calculated by integrating both types of current over the surface.

The explicit solution for the nonuniform component is extremely difficult because of very complicated and immense equations involved. The contribution of the nonuniform component is determined by analogy with the corresponding solution for a strip. This leads to an

expression for the nonuniform contribution at wide angles in terms of modified diffraction coefficients representing the fields scattered by overlapping half-planes whose orientation is specified by the flash points obtained from a stationary phase analysis. The nonuniform portion of the total scattered field is thereby reduced to a summation of scattered fields rather than surface currents.

2.6 Numerical Methods

The starting point for the numerical method is the vector integral equation for the surface current. It is the most logical starting point because boundary and radiation conditions are automatically taken into account. To get our equation, we have to rewrite Eq. (12a)

$$\frac{1}{2} \vec{J}(\mathbf{r}) = \hat{n} \times \vec{H}^i(\mathbf{r}) + \frac{1}{4\pi} \int_S \hat{n}(\mathbf{r}) \times \{ \vec{J}(\mathbf{r}_1) \times \nabla \left(\frac{\exp(-ik|\mathbf{r}-\mathbf{r}_1|)}{|\mathbf{r}-\mathbf{r}_1|} \right) \} ds_1 \quad (22)$$

$\mathbf{r}, \mathbf{r}_1 \in S$

The next step is to divide the scattering surface in portions over each of which the amplitude and the phase of the surface field can be considered as approximately constant or as varying in an approximately known way. Thus the integral sign in Eq. (22) can be replaced by a summation sign and we get a set of linear algebraic equations to be solved numerically by a computer.

The set of algebraic equations can be reduced to a matrix form

$$[V] [J] = [H^i] \quad (23)$$

where $[V]$ is the known coefficient of the current $[J]$, while $[H^i]$ is the incident magnetic field. So $[J]$ can be found out by inverting matrix $[V]$.

Equation (22) can be solved by Moment method. For details see the book by Harrington [5]. A short review will be given here.

The idea of moment-method solutions is that the linear operator equation

$$L(f) = g \quad (24)$$

where L is a linear operator, g is some known driving fn. and f is to be determined, may be solved by first expanding f in a series of basis fns. f_n with unknown coefficients α_n , viz,

$$f = \sum_n \alpha_n f_n \quad (25)$$

Next, a set of weighting or testing fns. ω_m is chosen and an inner product taken in Eq. (24). After substitution of Eq. (25) into Eq. (24) the result is

$$\sum_n \alpha_n \langle \omega_m, Lf_n \rangle = \langle \omega_m, g \rangle \quad (26)$$

which may be written as

$$[l_{mn}] [\alpha_n] = [g_m] \quad (27)$$

This is easier to invert, and matrix inversion yields the solution for the unknown coefficients.

After finding the current on the surface we can use Eq. (16) or (17) to find the scattered field.

The numerical method is very effective when the shape of the body is complex. It is also well suited to problems in the low frequency and resonance regions.

If the dimensions of the scatterer are very large compared to the wavelength, the number of linear algebraic equations become very large and difficult to handle by presently available computers.

2.7 Geometrical Optics (GO)

The treatment of high-frequency diffraction to follow is restricted to perfectly conducting objects located in isotropic, homogeneous media.

We begin with Maxwell's equations

$$(\nabla^2 + k^2)\vec{E} = 0 \quad (9)$$

subject to the condition that

$$\nabla \cdot \vec{E} = 0 \quad (3)$$

The Luneberg-Kline expansion of the electric field for large ω is

$$\vec{E}(\vec{R}, \omega) = e^{-jk_0\psi(\vec{R})} \sum_{m=0}^{\infty} \frac{\vec{E}_m(\vec{R})}{(j\omega)^m} \quad (28)$$

in which \vec{R} is the position vector, and k_0 is the phase constant of empty space. Substituting (28) into (9) and (3) and equating like powers of ω , one obtains the eikonal equation

$$|\nabla\psi|^2 = n^2 \quad (29)$$

together with the first-order transport and conditional equations

$$\frac{\partial \vec{E}_0}{\partial s} + \frac{1}{2} \left(\frac{\nabla^2 \psi}{n} \right) \vec{E}_0 = 0 \quad (30)$$

$$\hat{s} \cdot \vec{E}_0 = 0 \quad (31)$$

plus higher order transport and conditional equations which do not concern us here. In the preceding equations

$$\hat{s} = \frac{\nabla\psi}{n} \quad (32)$$

is a unit vector in the direction of the ray path, and s is the distance along the ray path.

We are interested here in the solution at the high frequency limit, so the asymptotic approximation of \vec{E} reduces to

$$\vec{E}(s) \approx e^{-jk_0\psi(s)} \vec{E}_0(s) \quad (33)$$

Equation (30) is readily integrated to obtain

$$\vec{E}(s) = \vec{E}_0(0) e^{-jk_0\psi(0)} \sqrt{\frac{\rho_1 \rho_2}{(\rho_1 + s)(\rho_2 + s)}} e^{-jks} \quad (34)$$

in which $s = 0$ is taken as a reference point on the ray path, and

ρ_1 and ρ_2 are the principal radii of curvature of the wavefront at $s = 0$.

Employing the Maxwell curl equation

$$\nabla \times \vec{E} = -jkZ\vec{H} \quad (7)$$

we can obtain \vec{H} .

Equation (34) gives the propagation of \vec{E} in the space.

Let us find the GO field reflected from the point Q_R on a perfectly-conducting smooth curved surface S ; the distance between Q_R and the field point on the reflected ray is denoted by s . The outward directed unit normal vector at Q_R is \hat{n} , and \hat{s}^i and \hat{s}^r are unit vectors in the directions of incidence and reflection, respectively, as shown in Fig. 2.

From the boundary condition on the total electric field at Q_R on S

$$\hat{n} \times (\vec{E}^i + \vec{E}^r) = 0 \quad (35)$$

it can be shown that

$$\vec{E}_0^r(Q_R) = \vec{E}_0^i(Q_R) \cdot \underline{R} = \vec{E}_0^i(Q_R) \cdot [\hat{e}_{||}^i \hat{e}_{||}^r - \hat{e}_{\perp}^i \hat{e}_{\perp}^r] \quad (36)$$

where \hat{e}_{\perp}^i is a unit vector perpendicular to the plane of incidence, and $\hat{e}_{||}^i$, $\hat{e}_{||}^r$ are unit vectors parallel to the plane of incidence so that

$$\hat{e}_{||}^r = \hat{e}_{\perp}^i \times \hat{s} \quad (37)$$

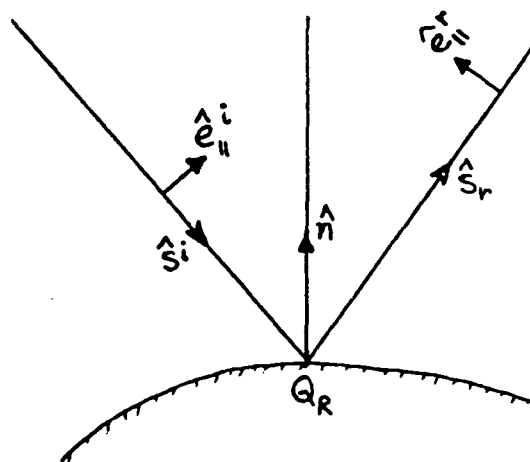


Fig. 2

In matrix notation the reflection coefficient has a form familiar for the reflection of a plane electromagnetic wave from a plane, perfectly conducting surface, namely

$$R = \begin{bmatrix} 1 & 0 \\ 0 & -1 \end{bmatrix} \quad (38)$$

This is not surprising if one considers the local nature of high-frequency reflection, i.e., the phenomenon for the most part depends on the geometry of the problem in the immediate neighborhood of Q_R . Note that the incident and reflected fields must be phase matched on S to satisfy Eq. (35), i.e.,

$$\psi^i(Q_R) = \psi^r(Q_R) \quad (39)$$

The above equality leads to the law of reflection, and it is also employed to obtain (36).

The geometrical optics reflected ray is

$$\vec{E}^{rg}(s) = \vec{E}^{ig}(Q_R) \cdot \sqrt{\frac{\rho_1^r \rho_2^r}{(\rho_1^r + s)(\rho_2^r + s)}} e^{-jks} \quad (40)$$

ρ_1^r and ρ_2^r are the principal radii of curvature of the reflected wavefront at Q_R . The general expressions have been given by Kouyoumjian [6].

For our study we are going to assume that the incident wave is a plane wave, and $s \gg \rho_1^r, \rho_2^r$ so that

$$\rho_1^r \rho_2^r = a_1 a_2 / 4 \quad (41)$$

and Eq. (40) becomes

$$\vec{E}^{rg}(s) = \vec{E}^{ig}(Q_R) \cdot R \sqrt{a_1 a_2} \frac{e^{-jks}}{2s} \quad (42)$$

a_1 and a_2 are principal radii of curvature of the surface S at Q_R .

It should be noted that for ω sufficiently large the GO field requires no correction, i.e., the scattering phenomenon is entirely dominated by GO. This is the case for backscatter from smooth curved surfaces with radii of curvature very large in terms of a wave length.

2.8 Geometrical Theory of Diffraction (GTD)

Geometrical Optics fails to predict the scattering from edges and also in the shadow region. To overcome these limitations, Dr. Keller introduced a theory which is now known as Geometrical Theory of Diffraction. Keller [7-9] has shown how the diffracted field may be included in the high frequency solution as an extension of GO. The postulates of GTD are summarized as follows.

(1) The diffracted field propagates along rays which are determined by a generalization of Fermat's principle to include points on the boundary surface in the ray trajectory.

(2) Diffraction like reflection and transmission is a local phenomenon at high frequencies, i.e., it depends only on the nature of the boundary surface and the incident field in the immediate neighborhood of the point of diffraction.

(3) The diffracted ray propagates along its ray such that
(a) power is conserved in a tube (or strip of rays)

(b) The phase delay along the ray path equals the product of wave number of the medium and the distance.

Diffracted rays are initiated at points on the boundary surface where the incident GO field is discontinuous. Examples of such points are edges, vertices and points at which the incident ray is tangent to a smooth curved surface. The diffracted rays like the GO rays follow paths which make the optical distance between the sourcepoint and the field point an extremum, usually a minimum.

Let us consider the field radiated from a point source at O , and observed at P in the presence of a perfectly conducting wedge, as shown in Fig. 3, where the rays are projected on a plane perpendicular to the edge at the point of diffraction Q_E .

Applying the generalized Fermats principle, the distance along the ray path $OQ_E P$ is a minimum and the law of edge diffraction

$$\hat{s}' \cdot \hat{e} = \hat{s} \cdot \hat{e} \quad (43)$$

results. Here \hat{e} is a unit vector directed along the edge, and \hat{s}' and \hat{s} are unit vectors in the directions of incidence and diffraction, respectively. Eq. (43) also follows from the requirement that the incident and diffracted fields be phase matched along the edge. If the incident ray strikes the edge obliquely, making an angle β'_0 with the edge, as shown in Fig. 4, diffracted rays lie on the surface of a cone whose half angle is equal to β'_0 . The position of the diffracted ray on this conical surface is given by angle ϕ , and the direction of the ray incident on the edge, by the angles ϕ' and β'_0 .

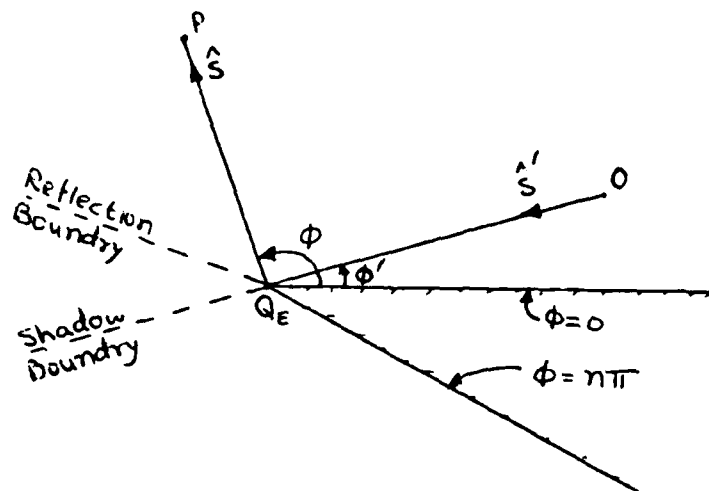


Fig. 3

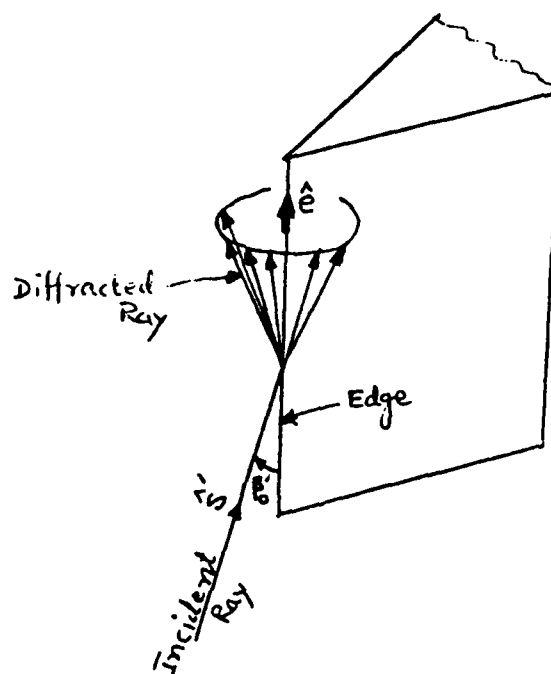


Fig. 4

It has been shown by Kouyoumjian [6] that the expression for the electric field of the edge diffracted ray is

$$\vec{E}^d(s) = \vec{E}^i(Q_E) \cdot \underline{D}(\phi, \phi', \beta'_0) \sqrt{\frac{\rho}{s(\rho+s)}} e^{-jks} \quad (44)$$

in which $\underline{D}(\phi, \phi', \beta'_0)$ is the dyadic edge diffraction coefficient, ρ is the distance between the caustics, one is the point of diffraction itself and the second caustic of the diffracted ray is away from the surface. The dyadic diffraction coefficient for a perfectly conducting wedge has been obtained by Kouyoumjian and Pathak [10]. They found out \underline{D} from the asymptotic solution of canonical problems, which in this case involves the illumination of the wedge by plane, cylindrical, conical, and spherical waves. The solution of these canonical problems serves as a basis for deducing the dyadic diffraction coefficient for arbitrary wavefront illumination and for the more general case where there are curved edges and curved surfaces.

Let us introduce an edge-fixed plane of incidence containing the incident ray and the edge and a plane of diffraction containing the diffracted ray and the edge. The unit vectors $\hat{\phi}'$ and $\hat{\phi}$ are perpendicular to the edge fixed plane of incidence and the plane of diffraction, respectively. The unit vectors $\hat{\beta}'_0$ are $\hat{\beta}_0$ parallel to the edge fixed plane of incidence and the plane of diffraction respectively, and

$$\hat{\beta}'_0 = \hat{s}' \times \hat{\phi}' \quad , \quad \hat{\beta}_0 = \hat{s} \times \hat{\phi} \quad (45)$$

Thus the coordinates of the diffracted ray (s, β_0, ϕ) are spherical coordinates and so are the coordinates of the incident ray (s', β_0', ϕ') except that the incident (radial) unit vector points toward the origin Q_E . These ray fixed-fixed coordinates and their unit vectors are shown on Fig. 5 and Fig. 6.

If the dyadic diffraction coefficient is expressed in an edge fixed coordinate system, it is found to be the sum of seven dyads. In matrix notation this means that the diffraction coefficient is a 3×3 matrix with seven non-vanishing elements, instead of the 2×2 diagonal matrix which may be used to represent the diffraction coefficient in the ray-fixed coordinate system. In this sense the ray-fixed coordinate system is the natural coordinate system of the problem.

For each type of illumination mentioned previously, it is shown by Pathak and Kouyoumjian [11] that the dyadic diffraction coefficient can be represented simply as the sum of two dyads, if the ray-fixed coordinates mentioned in the preceding paragraph are used.

$$\underline{D}(\phi, \phi', \beta_0') = -\hat{\beta}_0' \hat{\beta}_0 D_s(\phi, \phi', \beta_0') - \hat{\phi}' \hat{\phi} D_h(\phi, \phi', \beta_0') \quad (46)$$

where D_s is the scalar diffraction coefficient for the acoustically soft (Dirichlet) boundary condition at the surface of the wedge, and D_h is the scalar diffraction coefficient for the acoustically hard (Neumann) boundary condition.

Expressions for the scalar diffraction coefficients which are valid at all points away from the edge are

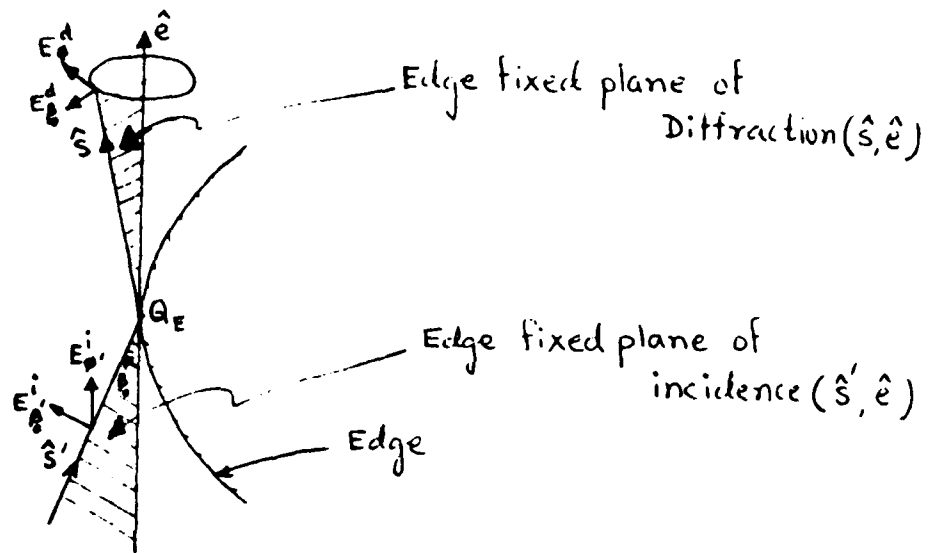


Fig. 5

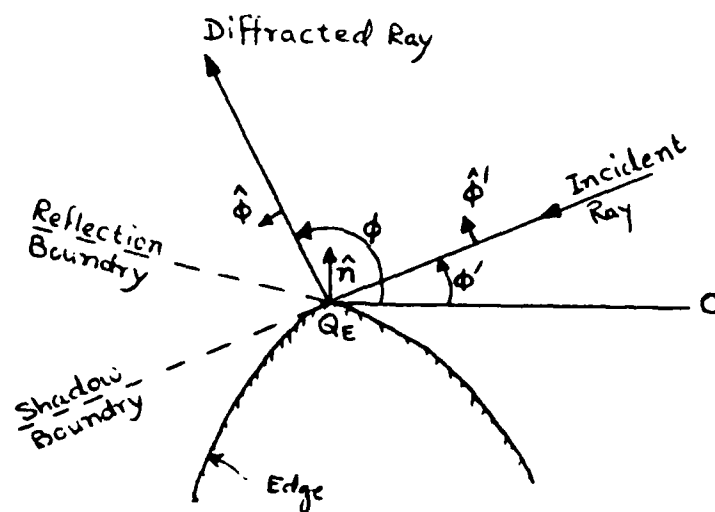


Fig. 6

$$D_{sh} = \frac{e^{-j\frac{\pi}{4}}}{2n\sqrt{2\pi k} \sin \beta_0'} \times \left\{ \cot\left(\frac{\pi+\alpha^-}{2n}\right) F(kL^i a^+(\alpha^-)) \right. \\
+ \cot\left(\frac{\pi-\alpha^-}{2n}\right) F(kL a^-(\alpha^-)) + [\cot\left(\frac{\pi+\alpha^+}{2n}\right) F(kL^{r_0} a^+(\alpha^+)) \\
+ \cot\left(\frac{\pi-\alpha^+}{2n}\right) F(kL^{r_n} a^-(\alpha^+))] \left. \right\} \quad (47)$$

$$\text{where } \alpha^+ = \phi + \phi' \quad (48)$$

$$\alpha^- = \phi - \phi' \quad (49)$$

$$F(X) = 2j|\sqrt{X}| e^{-jX} \int_{|\sqrt{X}|}^{\infty} e^{-j\tau^2} d\tau \quad (50)$$

If X is greater than 10 then $F(X) \approx 1.0$.

The large argument of the transition $f_n, X = kL^i a^+(\alpha^+)$ is KL^{i/r_0} , where L^{i/r_0} is a distance parameter which will be given later.

Let $\phi^+ \phi' = \alpha^+$, then

$$a^+(\alpha^+) = 2 \cos^2\left(\frac{2n\pi N^+ - \alpha^+}{2}\right) \quad (51)$$

in which N^+ are the integers which most nearly satisfy the equations

$$2\pi n N^+ - \alpha^+ = \pi \quad (52)$$

$$2\pi n N^- - \alpha^- = -\pi \quad (53)$$

$a^{\pm}(\alpha^{\pm})$ is a measure of the angular separation between the field point and a shadow or reflection boundary. The + or - superscripts are associated with the integers N^+ and N^- , respectively, which are defined by Eq. (52) and (53). For exterior edge diffraction ($1 < n < 2$) $N^+ = 0$, or 1, and $N^- = -1$, 0, or 1.

The distance parameter L can be found by imposing the condition that the total field (the sum of GO field and the diffracted field) be continuous at shadow or reflection boundaries.

$$L^i = \frac{S(\rho_e^i + s) \rho_2^i \rho_1^i \sin^2 \beta_0'}{\rho_e^i (\rho_1^i + s) (\rho_2^i + s)} \quad (54)$$

$$L^r = \frac{s(\rho_e^r + s) \rho_2^r \rho_1^r \sin^2 \beta_0'}{\rho_e^r (\rho_1^r + s) (\rho_2^r + s)} \quad (55)$$

where ρ_1^r and ρ_2^r are the principal radii of curvature of the reflected wavefront at Q_E , and ρ^r is the distance between the caustics of the diffracted ray in the direction of the reflection. ρ_1^i and ρ_2^i are the principal radii of curvature of the incident wavefront at Q_E , and ρ_e^i is the radius of curvature of incident wavefront in the edge fixed plane of incidence. The additional superscripts 0 and n on L in Eq. (47) denote that the radii of curvature (and caustic distance ρ) are calculated at the reflection boundaries $\pi - \phi'$ and $(2n-1)\pi - \phi'$, respectively. In the far zone where $s \gg \rho$ and the principal radii of curvature ρ_2 and ρ_2 of the incident and reflected wavefronts at Q_E , Eq. (54) and (55) simplify to

$$L = \frac{\rho_1 \rho_2 \sin^2 \beta_0'}{\rho} \quad (56)$$

The appropriate superscripts are omitted here for the sake of simplicity.

The caustic distance ρ can be calculated employing differential geometry. It is

$$\frac{1}{\rho} = \frac{1}{\rho_e} - \frac{\hat{n}_e \cdot (\hat{s} - \hat{s}_0)}{a \sin^2 \beta_0} \quad (57)$$

\hat{n}_e is the unit vector normal to the edge at Q_E and directed away from the center of curvature. a is the radius of curvature of the edge at Q_E , $a > 0$.

In summary, to calculate the diffraction from a curved edge, the scalar diffraction coefficients from Eq. (47) are substituted into Eq. (46) and the resulting dyadic diffraction coefficient is substituted into Eq. (44). The caustic distance ρ is calculated from Eq. (57). In matrix notation the diffracted electric field takes the form

$$\begin{bmatrix} E_{\beta_0}^d \\ E_{\phi}^d \end{bmatrix} = \begin{bmatrix} -D_s & 0 \\ 0 & -D_h \end{bmatrix} \begin{bmatrix} E_{\beta_0}^i \\ E_{\phi}^i \end{bmatrix} \cdot \sqrt{\frac{\rho}{s(\rho+s)}} e^{-jks} \quad (58)$$

The expression for vertex or corner diffraction of the electric field is

$$\vec{E}^d(s) = \vec{E}^i(Q_v) \cdot \underline{D}(\theta, \phi, \theta', \phi') \frac{e^{-jks}}{s} \quad (59)$$

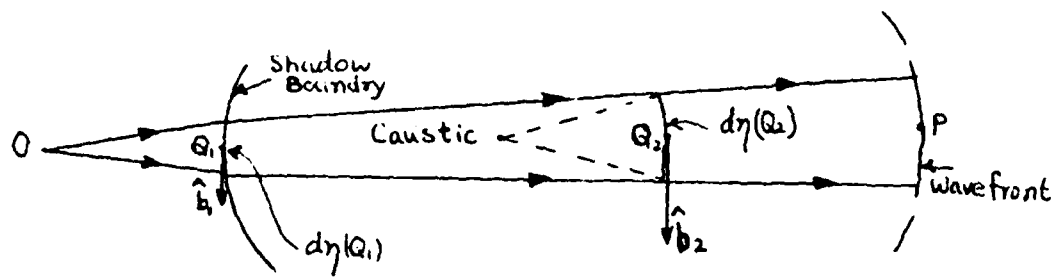
where $\underline{D}(\theta, \phi, \theta', \phi')$ is the vertex diffraction coefficient. Very little work has been done on the high-frequency diffraction by vertices.

When an incident ray strikes a smooth, curved perfectly conducting surface at grazing incidence, i.e., at the shadow boundary, a part of the energy is diffracted into the shadow region. Let us consider the field radiated by the source 0 and observed at p in the shadow region as shown in Fig. 7 and Fig. 8.

To satisfy the generalized Fermats principle, the surface ray must be a geodesic curve. Also it is required that the incident and diffracted fields are phase matched to the surface ray field at Q_1 and Q_2 . It is assumed that the surface rays are torsionless, i.e., \hat{b} does not change direction along the surface ray. Kouyoumjian [6] has given the following expression for surface diffraction.

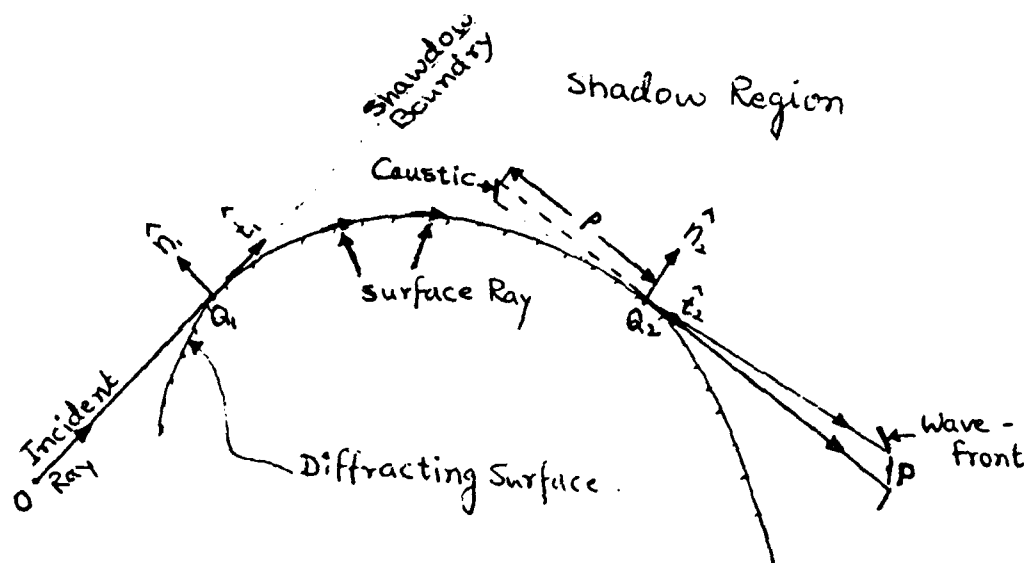
$$\vec{E}^d(p) = \vec{E}^i(Q_1) = [\hat{n}_1 \hat{n}_2 F + \hat{b}_1 \hat{b}_2 G] \sqrt{\frac{\rho}{s(\rho+s)}} e^{-jks} \quad (60)$$

In the same reference Kouyoumjian [6] has shown how to find F and G and ρ is found from Eq. (57). Calculating F and G is quite involved, and interested readers are requested to see reference [6].



TOP VIEW

Fig. 7



SIDE VIEW

Fig. 8

CHAPTER THREE

THE CHOICE OF METHOD

Recently there has been considerable interest in the integral equation formulation of the radiation problem, and its solution by the moment method. Arbitrary shapes can be handled by this method, but in general, numerical results are restricted to objects not large in terms of a wavelength, because of the limitations of present day computers.

Tsai, Dudley and Wilton [12] have used the moment method to solve the vector magnetic field integral equation, and thus calculated electromagnetic scattering by a three dimensional rectangular box. They have shown that using an 8x8 sampling on each face of a cube would require 768x768 matrix to be solved. Looking at this enormous problem for such a simple object as a cube, we shelve this method for the time being until some mathematical breakthrough or the computer improvement is achieved in solving such problems.

Now we are left with two methods for calculating the scattered field. One is Physical Optics combined with Physical Theory of Diffraction and the other is Geometrical Optics combined with Geometrical Theory of Diffraction. The results obtained by PO are frequency dependent, and it is therefore possible that PO provides a more accurate estimate of the scattering. But it has been noted that PO in general fails to satisfy the reciprocity theorem everywhere except in the direction of a specular return. Also no rigorous justification for PO approximations have been established. PTD has a lot

of potential to be a leading method in predicting diffraction, but a lot of work will have to be done. Thus if PTD is to be judged by the description given by Ufimtsev [4], it is less complete than GTD and, moreover, does not give the correct second order diffraction for strips and disks.

According to Knott, Thomas and Senior [13] GTD is as good as any other method. It has some advantages and some disadvantages. The serious disadvantage being that it predicts infinite field at the ray caustic. So as long as we keep away from the ray caustic, it is an elegant method with the conceptual simplicity. Also R. Mittra and W. L. Ko [14] have concluded in this reference that GO solution is a very good approximation to the exact solution except in the neighborhood of the forward scattering direction. Also, it has been found in many cases GO and GTD has worked surprisingly well on radiating objects as small as a wavelength or so in extent.

Since we are interested only in the backscattering, we conclude that at the present time the best practical method to model the scattering field from a 3-D object is the Geometrical Optics in combination with Geometrical Theory of Diffraction.

CHAPTER FOUR

APPLICATIONS

Application of Geometrical Optics and the Geometrical Theory of Diffraction to calculate the backscattered field from 3-D objects is a straightforward matter. The first step is to find out all scattering points on the object. This is purely an exercise in geometry.

Since we are interested only in the backscattered field, it is easier to find the scattering points. The direction of the scattered ray must be exactly opposite to the incident ray. The points which satisfy this constraint are the specular points.

The second step is to apply the necessary equations that are developed before, at these scattering points. The final step is to sum up all the scattered field at the given position to get the total field.

We are going to apply this methodology to calculate the backscattered field from a sphere which has been studied extensively and from a spherical segment.

4.1 Back Scattering from a Sphere

A great deal of research has been done on the EM backscatter from the sphere since it has the simplest geometry. The exact closed form mathematical solution for the EM backscatter is known. A theoretical derivation of the field scattered by perfectly conducting

spheres is given by Harrington [15]. Chapter 10 of Electromagnetic and Acoustic Scattering by Simple Objects [16] gives the pertinent equations to calculate the exact EM backscatter from spheres. Rheinstei[n] [17] and Bechtel [18] have tabulated the numerical results.

The purpose of picking up the sphere to calculate the back-scattering is to test the practicality of our equations with the known results. The situation is shown in Fig. 9.

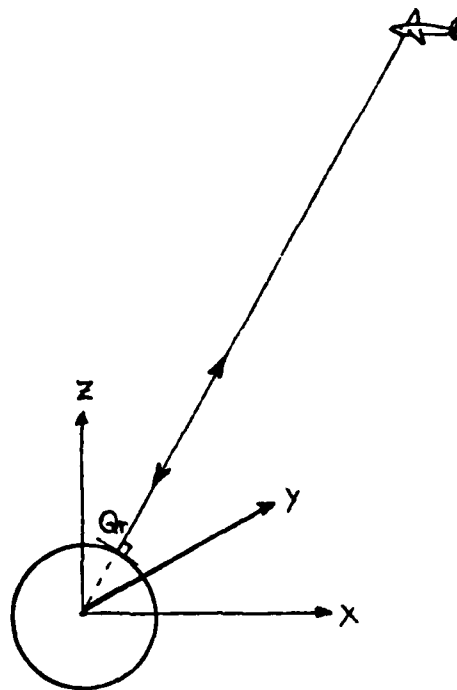
In this case we will have backscattering due to reflection and due to surface diffraction. But we will neglect the contribution of the surface diffraction since it is quite small compared to that of reflection. Dimensional considerations show that the coefficient of surface diffraction decreases exponentially with decreasing λ , and our mathematical model hinges on the assumption that the frequency of EM radiation is very high. Therefore, at high frequencies the return from the surface wave will be very weak.

The specular point Q_T will lie at the intersection of the surface of the sphere and the line joining the center of the sphere and the aircraft radar for the obvious reason that the incident ray will be orthogonal to the surface, so that the reflected ray will be exactly in the opposite direction.

The equation to be applied is the GO formulation and we get

$$\vec{E}^{rg}(s) = -\vec{E}_0 \sqrt{\frac{\rho_1 \rho_2}{(\rho_1 + s)(\rho_2 + s)}} \sqrt{\frac{a_1 a_2}{4}} \frac{e^{-jk2s}}{s} \quad (61)$$

$\vec{E}^{rg}(s)$ is the scattered field received at the antenna. \vec{E}_0 is the EM field at the origin of antenna.



Back Scatter from a Sphere

Fig. 9

ρ_1 and ρ_2 are the principal radii of curvature of the wavefront at the origin of the antenna and it is assumed to be known. a_1 and a_2 are the principal radii of curvature of the surface at the point of reflection, and in our case it is equal to the radius of the sphere. s is the distance between the antenna and the specular point. k is the wave number.

4.2 Back Scattering from a Spherical Segment

Now we are going to calculate the backscattered field using GO and GTD.

The situation that we will be considering is as follows. An airplane in the sky is trying to detect objects like cars, tanks, etc. which are on the ground with its radar. The radar emits the EM signals and then gathers the scattered signals. Since the velocity of the plane is much lower than that of EM signals, we can assume that the whole situation is static and the signals that the radar receives are the backscattered signals. We will also assume the radar to be a point source and a point receiver because the distance between the object and the radar is much larger than the dimensions of the radar. We will also assume that the object is perfectly conducting. Let us take the object to be a car. To make the problem tractable, we will say the car resembles a spherical segment sitting on the ground. The situation has been depicted in Fig. 10.

To summarize, the simplifications that we have made

- (i) The object is perfectly conducting.

- (ii) The object is a spherical segment.
- (iii) The object is very large compared to the wavelength of the radiation.
- (iv) The radiation is monochromatic and the surrounding of the object is almost a vacuum.
- (v) The frequency of the signal is quite high.
- (vi) The situation is static.

We will not consider backscattering due to surface diffraction for the following reason. Dimensional considerations show that the edge diffraction coefficients are proportional to $\lambda^{\frac{1}{2}}$ and tip or vertex diffraction coefficients to λ . The field diffracted around a curved surface decreases exponentially with decreasing λ and is consequently weaker than that diffracted by an edge for low values of λ [9]. This is even more true in the case of backscattering. To substantiate our claim further, we refer to the research done by Weiner [19]. He confined his studies only to a hemisphere with a nose on incidence. He also conducted some experiments. He concluded that the GTD appeared to give the correct magnitude and frequency dependence for the singly diffracted return. However, the doubly diffracted return is considerably weaker than diffraction theory would predict and decreases rapidly with frequency. Surface wave return is the weakest of all and it also decreases rapidly with the increasing frequency.

The origin of the coordinate axis coincides with the center of an imaginary sphere of which the spherical segment is a part. Let D be the diameter of the imaginary sphere and let the height of the

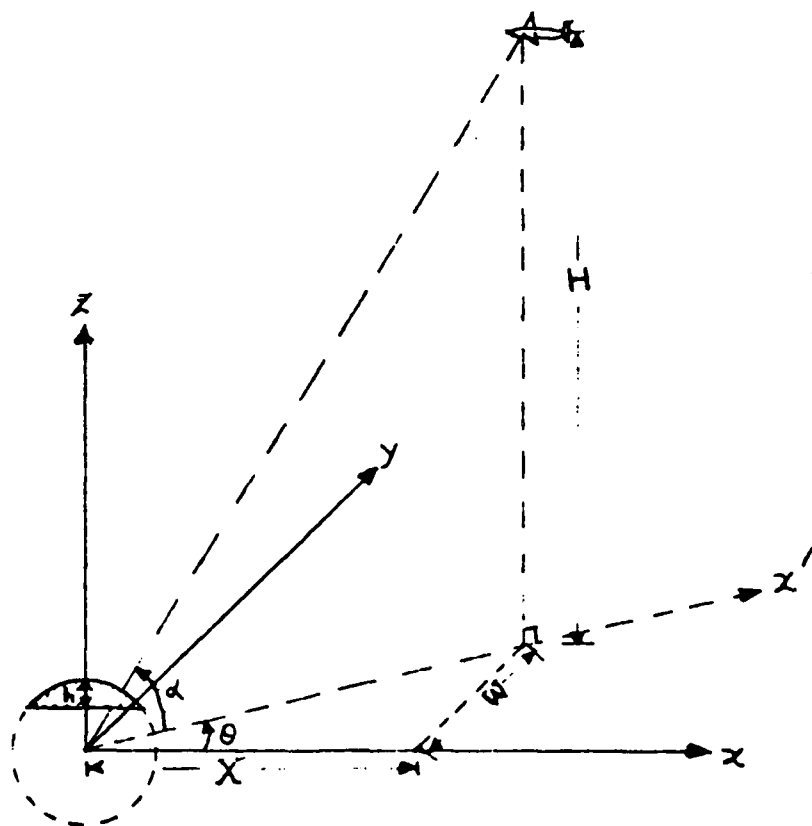


Fig. 10

spherical segment be h . The flat surface of the spherical segment lies parallel to the XY plane.

When the radiated beam covers the object, we will have scattering from the object. At all times there will be at least one scattering point on the edge. Additional scattering points will come into the picture depending upon the relative position of the aircraft and the spherical segment. In one situation (see Fig. 12) the scattering will be from the edge only.

In another situation (see Fig. 12) there will be two scattering points--one point will be on the edge, while the other is on the smooth curved surface.

In the third situation (see Fig. 13) there will be three scattering points, two points are located on the edge and the third point is on the smooth curved surface. We will not consider the nose on incidence because it is a remote case.

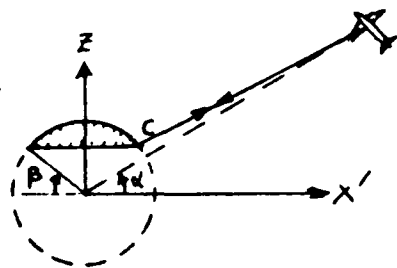
First let us give the conditions under which these additional scattering points occur.

Let the positional vector of the aircraft be \vec{R}

$$\vec{R} = X\hat{i} + W\hat{j} + H\hat{k} \quad (62)$$

Therefore, the angle α between the line joining the aircraft with the origin and its projection on the ground (XY plane) is given by

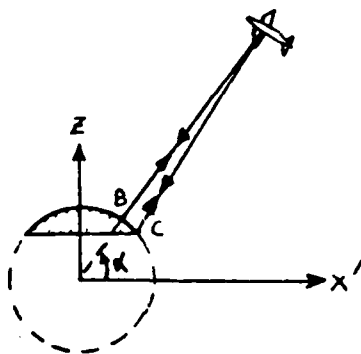
$$\alpha = \text{Arc tan} \left(\frac{H}{\sqrt{X^2 + W^2}} \right) \quad (63)$$



Only one pt. is scatterer.

SKEW VIEWS

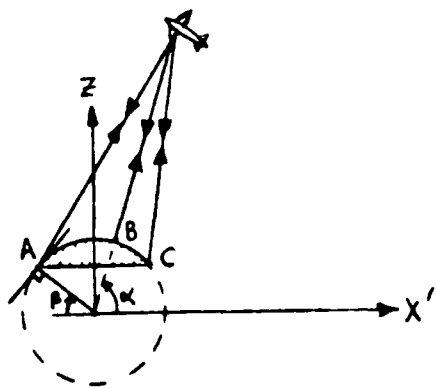
Fig. 11



Pt B is a reflection pt.
and pt. C is a scattering pt.

SKEW VIEWS

Fig. 12



Pt. A and Pt C are scattering
pts and pt. B is a reflection pt

SKEW VIEW

Fig. 13

The angle β between the line joining any point on the curved edge with the origin and its projection on the ground is given by

$$\beta = \text{Arc sin} \left(\frac{D/2-h}{D/2} \right) \quad (64)$$

Whenever the radiation covers the object we will have backscatter at least from a point on the curved edge which is closest to the aircraft. This is so because the incident radiation must be perpendicular to the edge in order to get the backscatter.

We will have reflection from the curved surface of the spherical segment in addition to the diffraction from the edge when

$$\beta < \alpha \leq \pi/2 \quad (65)$$

The point of reflection will lie at the intersection of the curved surface of the spherical segment and the line joining the radar with the origin; i.e., the incident and the reflected ray are perpendicular to the surface.

We can have one more scattering point on the curved edge. This scattering point must lie diametrically opposite to the first scattering point because the incident ray must be orthogonal to the tangent of the edge at that point to get the backscatter.

Let γ be the angle between the line joining the aircraft with point A and its projection on the ground.

$$\gamma = \text{arc tan} \left(\frac{H - \frac{D}{2} + H}{w} \right) \quad (66)$$

$$\text{where } W' = \sqrt{X^2 + W^2} + a' \quad (67)$$

a' is the radius of curvature of the edge and it is given by

$$a' = \sqrt{(D/2)^2 - (D/2 - h)^2} \quad (68)$$

We will have this additional scattering point when

$$(\frac{\pi}{2} - \beta) < \gamma \quad (69)$$

This can clearly be seen from Fig. 13.

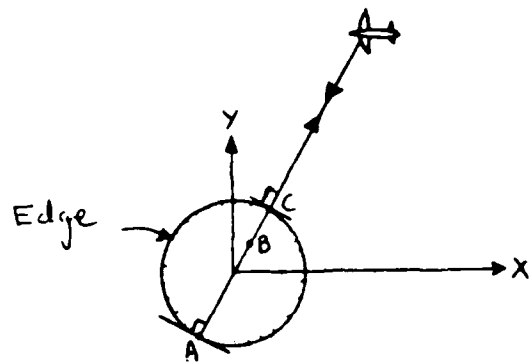
We conclude that if the condition given by Eq. (69) is satisfied, we will have diffraction from two points on the curved edge and reflection from one point on the surface. If only Eq. (65) is satisfied, then we will have scattering from one point on the edge and the reflection from the surface. Note that if Eq. (69) is satisfied, Eq. (65) is satisfied automatically. If the condition in Eq. (65) is not satisfied, then the scattering will be from one point on the edge only.

Let us consider the situation where there is diffraction from two points on the edge and the reflection from one point. Refer to Fig. 14.

We have the solution for the reflection from point B

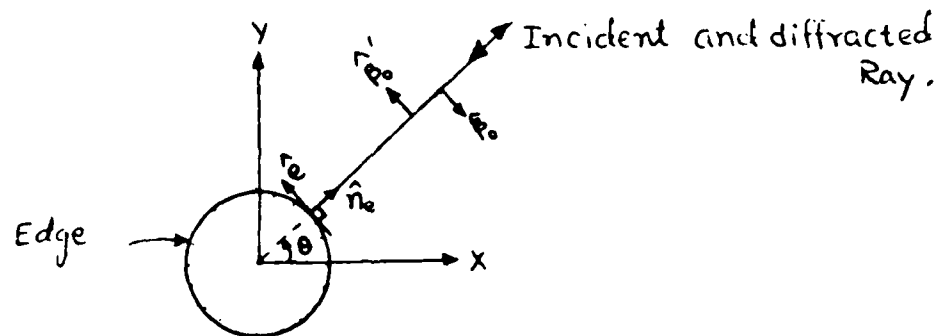
$$\vec{E}_B^{rg}(0) = -\vec{E}_0 \sqrt{\frac{\rho_1 \rho_2}{(\rho_1 + s_B)(\rho_2 + s_B)}} \cdot \frac{\sqrt{a_1 a_2}}{2} \frac{e^{-jk \cdot 2s_B}}{s_B} \quad (70)$$

$\vec{E}_B^{rg}(0)$ is the electric field returned to the aircraft antenna after the reflection at point B.



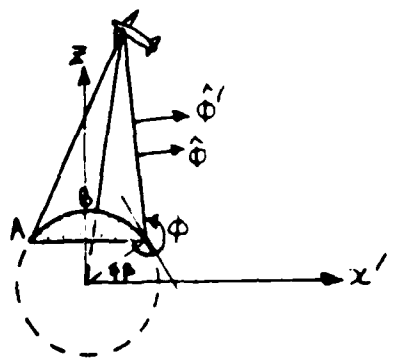
TOP VIEW

Fig. 14



TOP VIEW

Fig. 15



SKREW VIEW

Fig. 16

\vec{E}_0 is the originating field at the radar.

ρ_1 and ρ_2 are the principal radii of curvature at the point of origin of radiation and they are assumed to be known.

s_B is the distance between the antenna and the point B .

$$s_B = \sqrt{X^2 + W^2 + H^2} - D/2 \quad (71)$$

a_1 and a_2 are the radii of curvature of the reflected wavefront at B.

$$a_1 = a_2 = D/2 \quad (72)$$

$$k = 2\pi/\lambda \quad (73)$$

where λ is the wavelength.

Now let us consider the diffraction from point C which is the closest point on the edge from the antenna. Let \vec{R}_C be the positional vector of point C with respect to the origin.

$$\vec{R}_C = \frac{D}{2} [\cos\beta (\cos\theta \hat{i} + \sin\theta \hat{j}) + \sin\beta \hat{k}] \quad (74)$$

$$\theta = \arctan \left(\frac{W}{X} \right) \quad (75)$$

Consider Fig. 15 and Fig. 16.

Let us introduce an edge fixed plane of incidence containing the incident ray and the tangent of the edge at point C. Also consider the edge fixed plane of diffraction containing the diffracted ray and the tangent of the edge. Since the incident ray and the diffracted ray lie on the same line, both the planes are identical.

The unit vectors $\hat{\phi}'$ and $\hat{\phi}$ are perpendicular to the edge fixed plane. $\hat{\phi}'$ is associated with the incident ray while $\hat{\phi}$ is associated with the diffracted ray.

$$\hat{\phi} = \hat{\phi}' = \sin(\phi - \pi) [-\cos\theta \hat{i} - \sin\theta \hat{j}] + \cos(\phi - \pi) \hat{k} \quad (76)$$

$$\angle\phi = \arctan \left(\frac{H - \frac{D}{2} + h}{\sqrt{X^2 + W^2 - a^2}} \right) + \pi \quad (77)$$

The unit vectors $\hat{\beta}_0'$ and $\hat{\beta}_0$ are parallel to the edge fixed plane of incidence and diffraction. Also they are orthogonal to the incident and diffracted ray. \hat{e} is the unit vector tangential to the curved edge at the point C.

$$\hat{e} = \hat{\beta}_0' = -\hat{\beta}_0 = -\sin\theta \hat{i} + \cos\theta \hat{j} \quad (78)$$

$$\hat{s}' = \hat{\phi}' \times \hat{\beta}_0' \quad (79)$$

$$\hat{s} = \hat{\phi} \times \hat{\beta}_0 \quad (80)$$

\hat{s} is the unit directional vector of the diffracted ray.

The angle between the two surfaces which form the edge is given by

$$n\pi = 2\pi - \left(\frac{\pi}{2} - \text{Arc Sin} \left(\frac{D/2 - h}{D/2} \right) \right) \quad (81)$$

$$n = \frac{3}{2} + \frac{1}{\pi} \text{Arc Sin} \left(\frac{D/2 - h}{D/2} \right) \quad (82)$$

$\Gamma_{\beta_0'}^i(C)$ = The component of the electric field vector at point C in the direction of $\hat{\beta}_0'$.

$$\vec{E}_{\beta_0'}^i(C) = (\vec{E}_0 \cdot \hat{\beta}_0') \sqrt{\frac{\rho_1 \rho_2}{(\rho_1 + s_C)(\rho_2 + s_C)}} e^{-jks_C} \hat{\beta}_0' \quad (83)$$

s_C is the distance between the point C and the antenna.

$$s_C = \sqrt{\left[X - \frac{D}{2} \cos \beta \cos \theta\right]^2 + \left[W - \frac{D}{2} \cos \beta \sin \theta\right]^2 + [H - R \sin \beta]^2} \quad (84)$$

$\vec{E}_{\phi}^i(C)$ = The component of the incident electric field vector at point C in the direction of $\hat{\phi}'$.

$\vec{E}_{\beta_0}^d(OC)$ = The component of the electric field, diffracted from point C, returned to the antenna in $\hat{\beta}_0$ direction.

$$\vec{E}_{\phi}^i(C) = (\vec{E}_0 \cdot \hat{\phi}') \sqrt{\frac{\rho_1 \rho_2}{(\rho_1 + s_C)(\rho_2 + s_C)}} e^{-jks_C} \hat{\phi}' \quad (85)$$

$$\vec{E}_{\beta_0}^d(OC) = -D_s \vec{E}_{\beta_0}^i(C) \sqrt{\frac{\rho}{(s_C(\rho + s_C))}} e^{-jks_C} \quad (86)$$

where D_s is called the diffraction coefficient for the soft surface and ρ is caustic distance.

ρ is given by

$$\frac{1}{\rho} = \frac{1}{\rho_e^i} - \frac{\hat{n}_e \cdot (\hat{s}' - \hat{s})}{a'} \quad (87)$$

ρ_e^i is the radius of curvature of the incident wavefront in the edge fixed plane of incidence. Since the wavefronts are almost planar at point C

$$\frac{1}{\rho_e^i} \approx 0.0 \quad (88)$$

\hat{n}_e is the unit vector normal to the edge at C and directed away from the center of curvature.

$$\text{Therefore } \hat{n}_e \cdot (\hat{s}' - \hat{s}) = -2 \cos(\phi - \pi) \quad (89)$$

$\vec{E}_{\phi}^d(O_C)$ = The component of the electric field, diffracted from point C, returned to the antenna in $\hat{\phi}$ direction.

$$E_{\phi}^d(O_C) = -D_h \vec{E}_{\phi}^i(C) \sqrt{\frac{\rho}{s_C(\rho+s_C)}} e^{-jks_C} \quad (90)$$

D_h is called the diffraction coefficient for the hard surface.

The general expression for D_s and D_h is given by Eq. (47).

In this particular case

$$D_s = \frac{-e^{-j\pi/4}}{2n \sqrt{2\pi k}} \left[\frac{-2 \sin \frac{\pi}{n} F(2kL^i)}{\cos \frac{\pi}{n} - 1} + \left\{ \cot \left(\frac{\pi+2\phi}{2n} \right) F(kL^r_{o+}(2\phi)) + \cot \left(\frac{\pi-2\phi}{2n} \right) F(kL^r_{n-}(2\phi)) \right\} \right] \quad (91)$$

The upper sign goes with D_s , while the lower sign goes with D_h .

$F(\cdot)$ is called a transition fn. and for our purpose

$$F(\cdot) \approx 1.0 \quad (92)$$

The transition fn. is important at only very few points, especially when

$$\frac{\pi+2\phi}{2n} = \pi \quad (93)$$

At this particular value $F(\cdot)$ has different value than 1.0, but this is a solitary point. Therefore, for most practical case $F(\cdot) \approx 1.0$.

Then Eq. (91) simplifies to

$$D_{\frac{s}{h}} = \frac{e^{-j\pi/4}}{2n\sqrt{2\pi k}} \left[\frac{-2 \sin \pi/n}{\cos \pi/n - 1} + \left\{ \cot\left(\frac{\pi+2\phi}{2n}\right) + \cot\left(\frac{\pi-2\phi}{2n}\right) \right\} \right] \quad (94)$$

For the point A exactly the same procedure is to be used, except for the minor changes in the angles and distances.

Let \vec{R}_A be the positional vector of point A which is the farthest point on the edge from the antenna.

$$\vec{R}_A = \frac{D}{2} [\cos\beta(-\cos\theta \hat{i} - \sin\theta \hat{j}) + \sin\beta \hat{k}] \quad (95)$$

Let $\hat{\phi}_A'$ and $\hat{\phi}_A$ be the unit vectors perpendicular to the edge fixed plane at point A. $\hat{\phi}_A$ is associated with the incident ray at A, while $\hat{\phi}_A'$ is associated with the diffracted ray.

$$\hat{\phi}_A' = \hat{\phi}_A = \hat{\phi} \quad (96)$$

This is so because the radius of curvature of the edge is much smaller than the distance between the object and the antenna. Also since the incident ray and the diffracted ray have exactly opposite direction, the edge fixed planes are the same.

The unit vectors $\hat{\beta}_0'$ and $\hat{\beta}_0$ are parallel to the edge fixed plane of incidence and diffraction and they are the same as before.

$\vec{E}_{\beta_0'}^i(A)$ = The component of incident electric field vector at point A in the direction of $\hat{\beta}_0'$

$$\vec{E}_{\beta_0}^i(A) = (\vec{E}_0 \cdot \hat{\beta}_0) \sqrt{\frac{\rho_1 \rho_2}{(\rho_1 + s_A)(\rho_2 + s_A)}} e^{-jks_A} \hat{\beta}_0 \quad (97)$$

s_A is the distance between the point A and the aircraft antenna.

$$s_A = \sqrt{(X+D/2 \cos\beta \cos\theta)^2 + (W+D/2 \cos\beta \sin\theta)^2 + (H-D/2 \sin\beta)^2} \quad (98)$$

$\vec{E}_{\phi}^i(A)$ = The component of incident electric field vector at point A in the direction of $\hat{\phi}$

$$\vec{E}_{\phi}^i(A) = (\vec{E}_0 \cdot \hat{\phi}) \sqrt{\frac{\rho_1 \rho_2}{(\rho_1 + s_A)(\rho_2 + s_A)}} e^{-jks_A} \hat{\phi} \quad (99)$$

$\vec{E}_{\beta_0}^d(O_A)$ = Component of the diffracted electric field vector at the antenna in $\hat{\beta}_0$ direction.

$$\vec{E}_{\beta_0}^d(O_A) = -D_s' \vec{E}_{\beta_0}^i(A) \sqrt{\frac{\rho_A}{s_A(\rho_A + s_A)}} e^{-jks_A} \quad (100)$$

ρ_A is the distance between the caustic

$$\rho_A = \frac{a'}{2 \cos(\phi' - \pi)} \quad (101)$$

$$\phi' = 2\pi - \text{Arc tan} \left(\frac{H-D/2+h}{\sqrt{X^2+W^2} + a'} \right) \quad (102)$$

$\vec{E}_{\phi}^d(O_A)$ = The component of the electric field at the antenna, after the diffraction at point A, in the direction of $\hat{\phi}$.

$$\vec{E}_{\phi}^d(O_A) = -D_h' \vec{E}_{\phi}^i(A) \sqrt{\frac{\rho_A}{s_A(\rho_A + s_A)}} e^{-jks_A} \quad (103)$$

The edge diffraction coefficient D_s' and D_h' is given by

$$D_h' = \frac{-e^{-jk\pi/4}}{2n \sqrt{2\pi k}} \left[-\frac{2 \sin\pi/n}{\cos\pi/n-1} + \left\{ \cot\left(\frac{\pi+2\phi'}{2n}\right) + \cot\left(\frac{\pi-2\phi'}{2n}\right) \right\} \right] \quad (104)$$

The total scattered field returned to the antenna is given by

$$\vec{E}^d = \vec{E}_{\phi}^d(O_A) + \vec{E}_{\beta_0}^d(O_A) + \vec{E}_{\phi}^d(O_C) + \vec{E}_{\beta_0}^d(O_C) + \vec{E}_B^{rg}(O) \quad (105)$$

CHAPTER FIVE

HIERARCHY PLUS INPUT-PROCESS-OUTPUT (HIPO) CHARTS

We need to document the method that has been developed in order to facilitate an overview of the system and to determine program functions for coding purposes. One such technique used is called Hierarchy plus Input-Process-Output (HIPO) which is developed by IBM.

A typical HIPO package contains three kinds of diagrams.

They are

(i) Visual Table of Contents: This diagram contains the names and identification numbers of all the overview and detail HIPO diagrams in the package and relationship of the functions in a hierarchical fashion.

(ii) Overview diagrams: High level HIPO diagrams, called overview diagrams, describe the major functions and reference the detail diagrams needed to expand the functions to sufficient detail. The overview diagrams provide, in general terms, the inputs, processes, and outputs.

(iii) Detail diagrams: Lower level HIPO diagrams contain the fundamental elements of the package. They describe the specific functions, show specific input and output items, and refer to other detail diagrams.

For more detail information about HIPO charts, please refer to IBM manual [20].

See HIPO package in Appendix I.

CHAPTER SIX

DISCUSSION AND SUGGESTIONS

We discussed the merits and shortcomings of the three more popular methods of calculating scattering, namely Physical Optics (PO) together with Physical Theory of Diffraction (PTD), Numerical Methods, and Geometrical Optics (GO) in conjunction with Geometrical Theory of Diffraction (GTD). We made some assumptions like the scattering body is a perfectly conducting body surrounded by isotropic and homogeneous media, the radiations are monochromatic and have high frequency, the dimensions of the object are large compared to the wavelength, and the situation is static. After conducting an extensive literature survey, we came to a conclusion that GO combined with GTD is the most practical way of calculating scattering.

We applied GO and GTD to calculate backscatter from a sphere and from a spherical segment which is a simple representation of a car. We have given all the equations in detail for these cases and also we have given "Hierarchical plus Input-Process-Output" charts for the ease of overview and coding purposes. These examples show that GO and GTD have conceptual simplicity and they are rather easy to apply.

So far we restricted ourselves to the scattering from perfectly conducting surface in isotropic and homogeneous media. One can extend it to treat partially conducting bodies or bodies coated with dielectric material of the surrounding being inhomogeneous and anisotropic, or any combination of these. Also, there is a lot of work to be done

in the case of the vertex scattering. It is one of the challenging problems to find the diffraction coefficient for a vertex or tip diffraction. One can study the effects of lower frequency on the scattering. Also one can improve upon the other methods of the calculating scattering especially the numerical technique which is more promising.

REFERENCES

1. Stratton, J. A., Electromagnetic Theory, McGraw-Hill Book Co., New York, 1941.
2. Maue, A. W., "Zur Formulierung eines Allgemeinen Beugungsproblems durch eine Integralgleichung," Z. Physik 126, 601-618.
3. Rusch, W. V. T., Potter, P. D., Analysis of Reflector Antennas, Academic Press, New York, 1970.
4. Ufimtsev, P. Ya., "Method of edge waves in the physical theory of diffraction," Original in Russian, translations prepared by the U.S. Air Force Foreign Technology Division, Wright-Patterson Air Force Base, Ohio, released for public distribution September 7, 1971.
5. Harrington, R. F., Field Computation by Moment Methods, MacMillan, New York, 1968.
6. Kouyoumjian, R. G., Numerical and Asymptotic Techniques in Electromagnetics, R. Mittra (editor), Ch. 6, Springer-Verlag publication, Berlin, Germany, 1975.
7. Keller, J. B., Proc. Symposium on Microwave Optics, Part II, McGill University (1953), Astia Document AD 211500 (1959), 207-210.
8. Keller, J. B., Calculus of Variations and its Applications, L. M. Graves (editor), McGraw-Hill Book Co., New York, 1958, 27-52.
9. Keller, J. B., "Geometrical Theory of Diffraction," J. of Opt. Soc. of Am., 52, 116-130, 1962.
10. Kouyoumjian, R. G., and Pathak, P. H., "A Uniform Geometrical Theory of Diffraction for an Edge in a Perfectly Conducting Surface," Proc. of the IEEE, Vol. 62, 1448-1461, 1974.
11. Pathak, P. H., and Kouyoumjian, R. G., "The Dyadic Diffraction Coefficient for a Perfectly Conducting Wedge," Report 2183-4, Electrosience Laboratory, The Ohio State University, Columbus, Ohio, 1973.
12. Tsai, L. L., Dudley, and Wilton, D.R., "Electromagnetic Scattering by a Three-Dimensional Conducting Rectangular Box," J. of Appl. Physics, Vol. 45, No. 10, 4393-4400, 1974.

13. Knott, E. F., Thomas, B. A., and Senior, "Comparison of Three High-frequency Diffraction Techniques," Proc. of IEEE, Vol. 62, No. 11, 1468-1474, 1974.
14. Mittra, R., Ko, W. L., "An Approach to high-frequency scattering from smooth convex surfaces," IEEE Trans. on Antenna and Prop., Vol. AP-25, 781-788, Nov. 77.
15. Harrington, R. F., Time Harmonic Electromagnetic Fields, McGraw-Hill Book Co., 1961.
16. Bowman, Senior, Uslenghi, Electromagnetic and Acoustic Scattering by Simple Shapes, North-Holland Publishing Company, Amsterdam, 1969.
17. Rheinstein, J., "Tables of the amplitude and phase of the backscatter from a conducting sphere (Radius-Wavelength=0.01 to 19 in steps of .01)," MIT Lincoln Lab, Group report 22G-16, DDC-490-820, June 1963.
18. Bechtel, M. W., "Scattering Coefficients for the Backscattering of Electromagnetic Waves from Perfectly Conducting Spheres," Cornell Aeronautical Laboratory Report No. AP/RIS-1, Buffalo, New York.
19. Weiner, S. D., "Scattering by Edges: The Hemisphere," IEEE Trans. on Antenna and Prop., 709-710, 1967.
20. HIPO -- A Design Aid and Documentation Technique, Published by IBM Corp., Second Edition, May 1975.

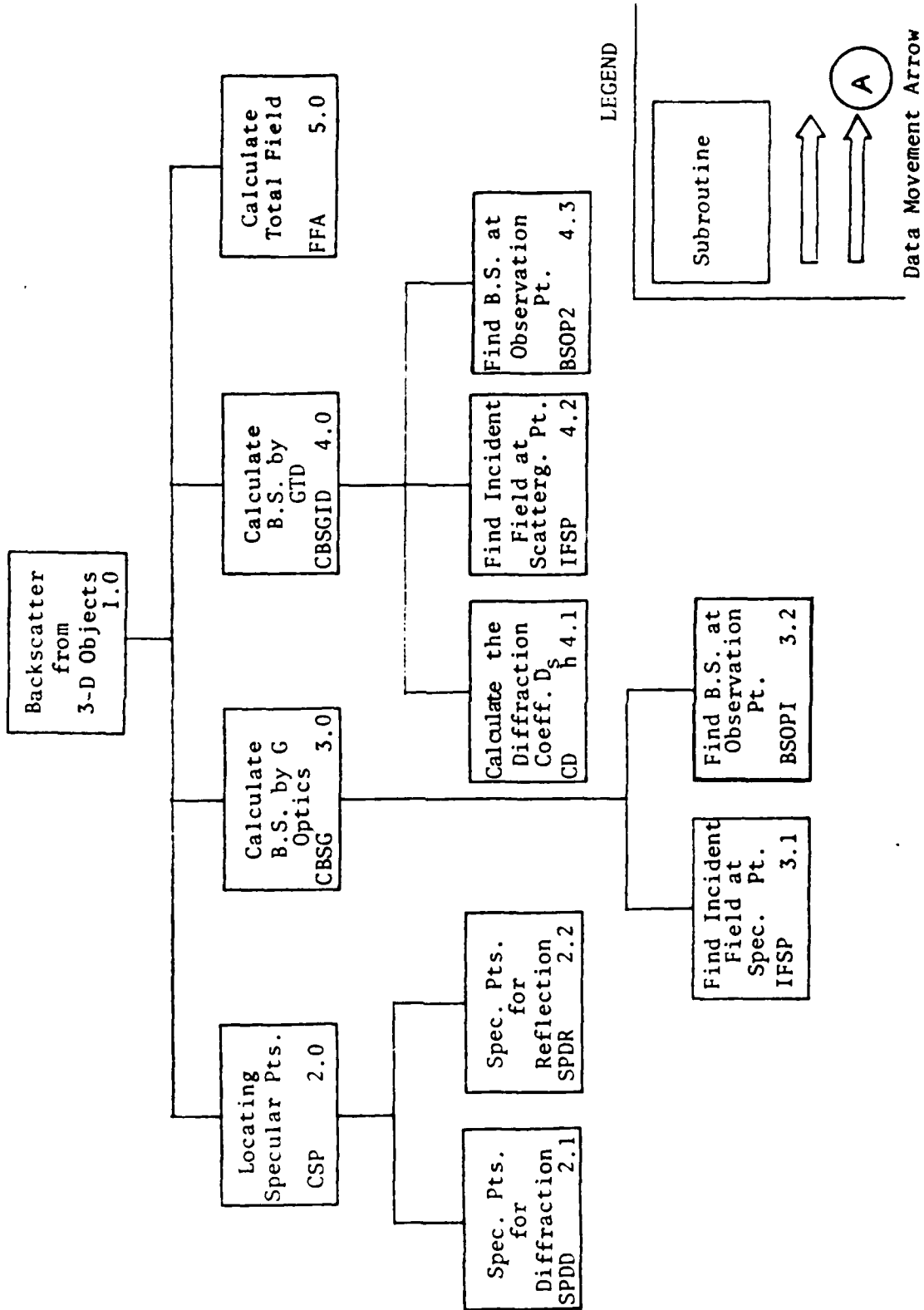
APPENDIX I

HIERARCHY PLUS INPUT-PROCESS-OUTPUT

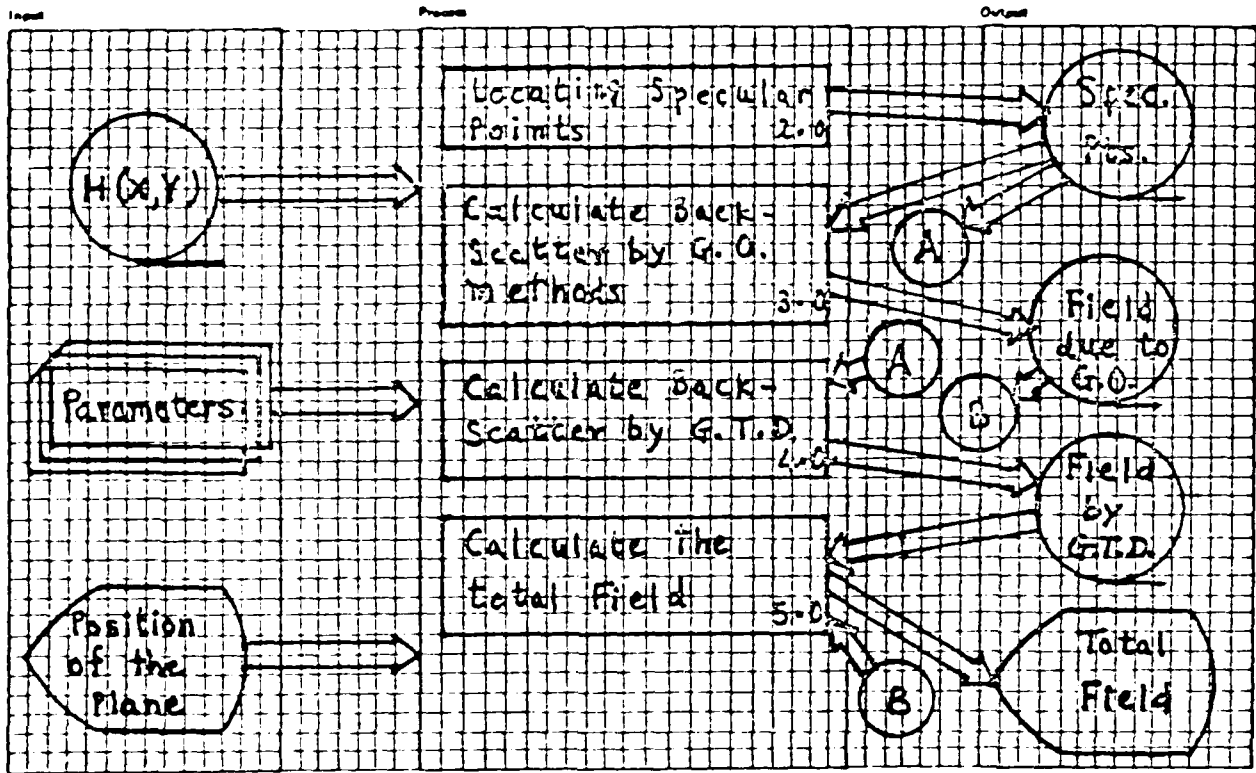
(HIPO) CHARTS

HIPO charts facilitate an overview of the system and determine the program functions for coding purposes.

The HIPO charts that follow contain a visual table of contents and overview diagrams of the problem that has been discussed.



Author A. P. Nayak 8, rue P. Segret B.S. from 3-D Objects Over 7/26/78 1 of 12
 Degree ID 1.0 Name _____ Drawn by B.S. Overview

[illegible]

HIPO WORKSHEET

CR 70-1070-0 U/M 025 -

2000-01-01

A.P.H. yalc

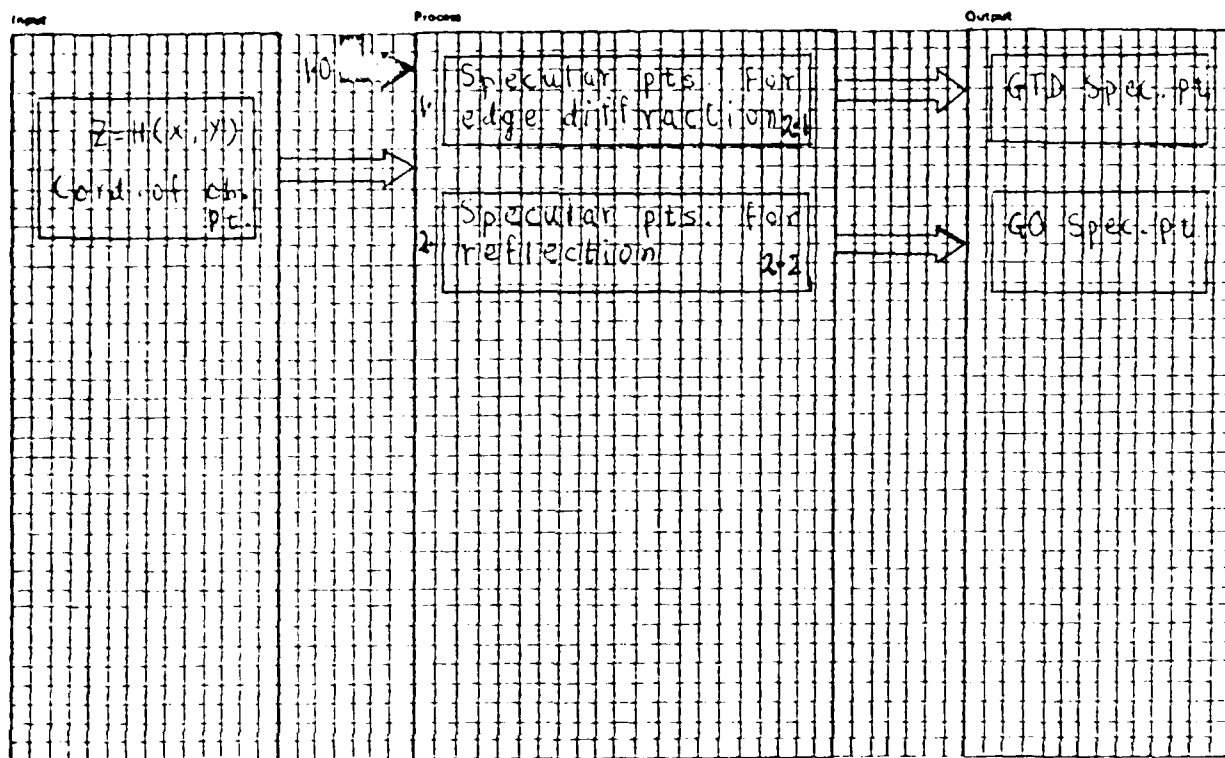
System Program 3.5 from 3-1 Objects

Date: 7/26/78 Pg: 2 of 12

2.0

Name: CSP

Description Calculate Specular Points



Extended Description

[illegible]

* Page 265, line 1: "The following table shows the results of the survey."

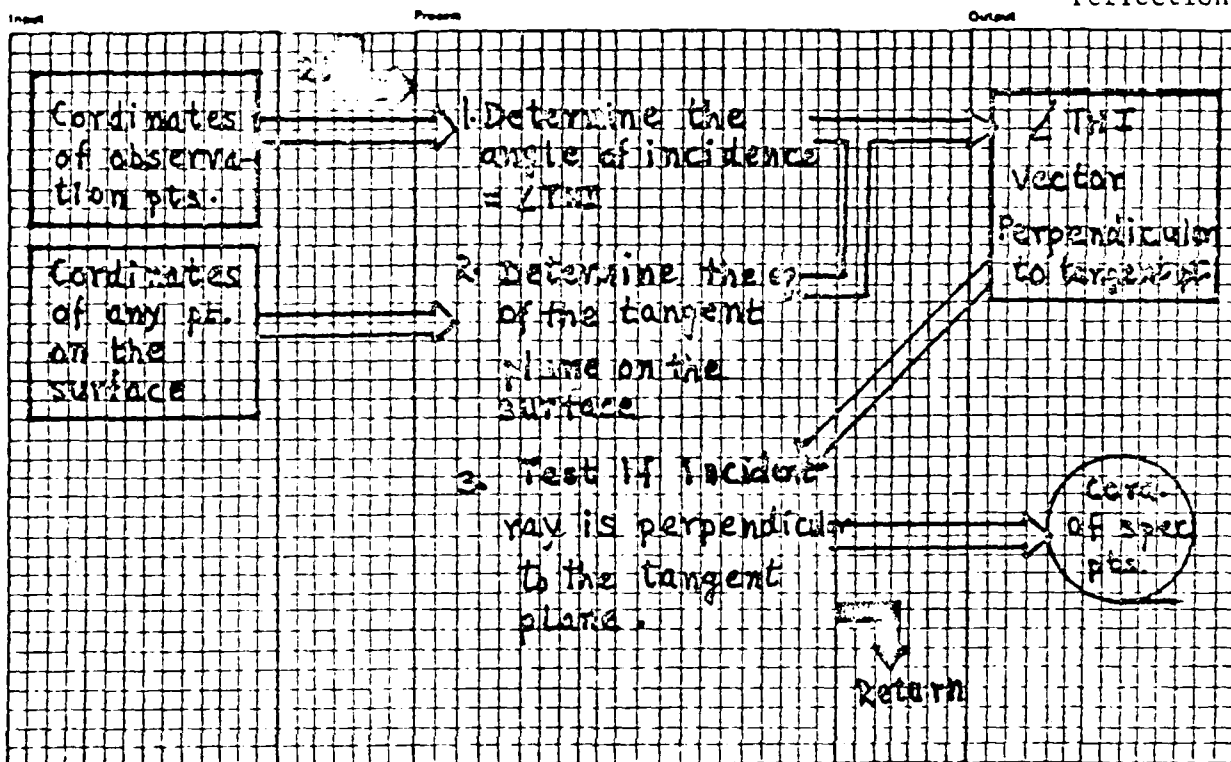
Diffraction



* The number of days per week by which the

Author A. P. Nayak System/Program B.S. from 3-D Objects Date 7/26/78 Page 4 of 12
 Diagram ID 22 Name SPDR Description Specular Pts. due to

reflection.

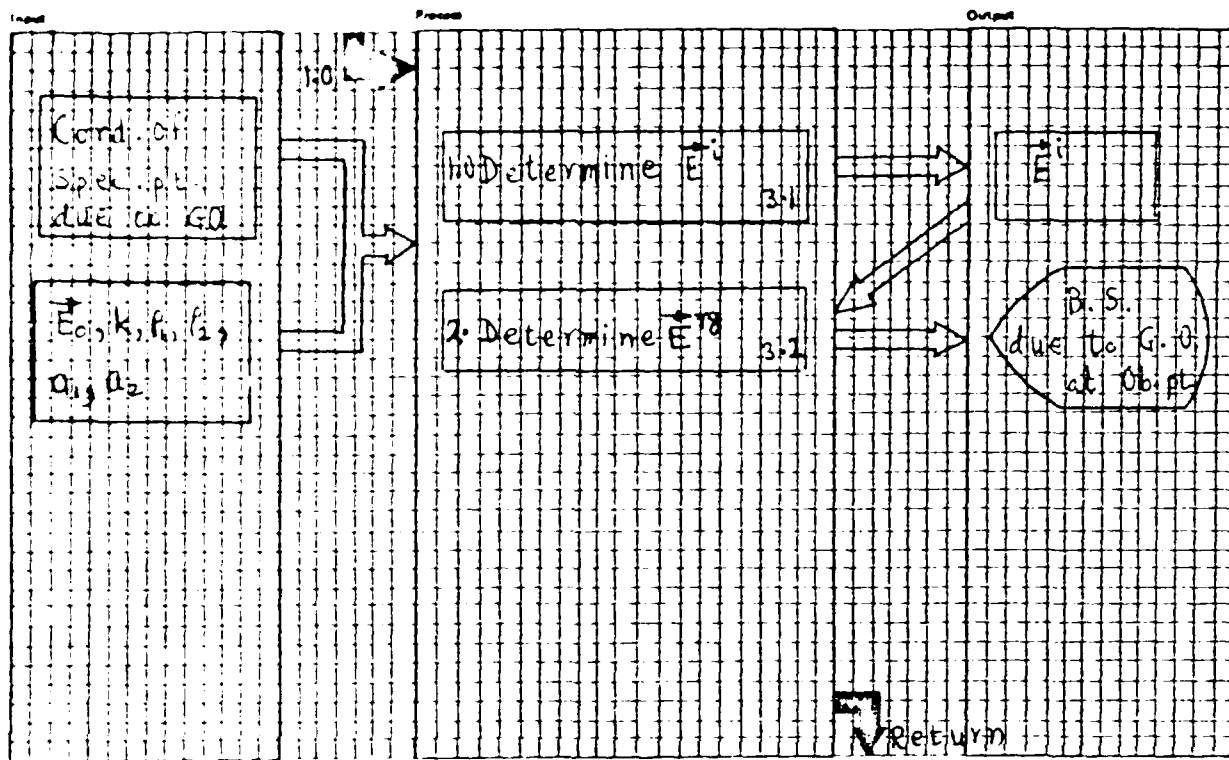
[illegible]

HIPO WORKSHEET

GA 70-1070-0 U/M 025 9

References

Author: A. P. Layman System/Program: B.S. from 3-2 objects Date: 7/26/78 Page: 2 of 12
 Organization: F.O. Name: CBCGO Description: Calculate B.S. by GO

[illegible]

* The number of fish captured may vary slightly

A. P. Nayak

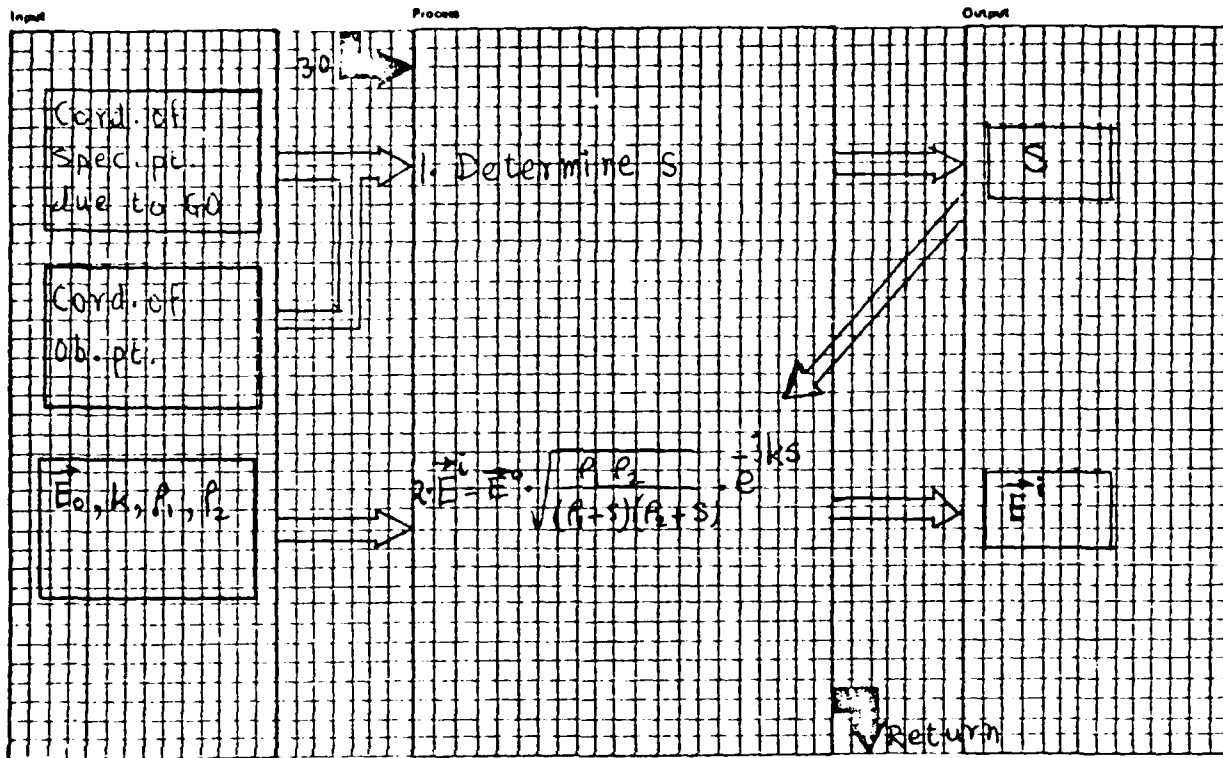
System/Program: B.S. from 3-D Objects

0.7/26/78, 6 12

Diagram ID: 3.1

Name: IFSP

Description: Incident Field at spec.pt

[illegible]

* The number of sheets printed may vary slightly.

Author: A.P. Nayak

System/Program: B.S. from 3-D Objects

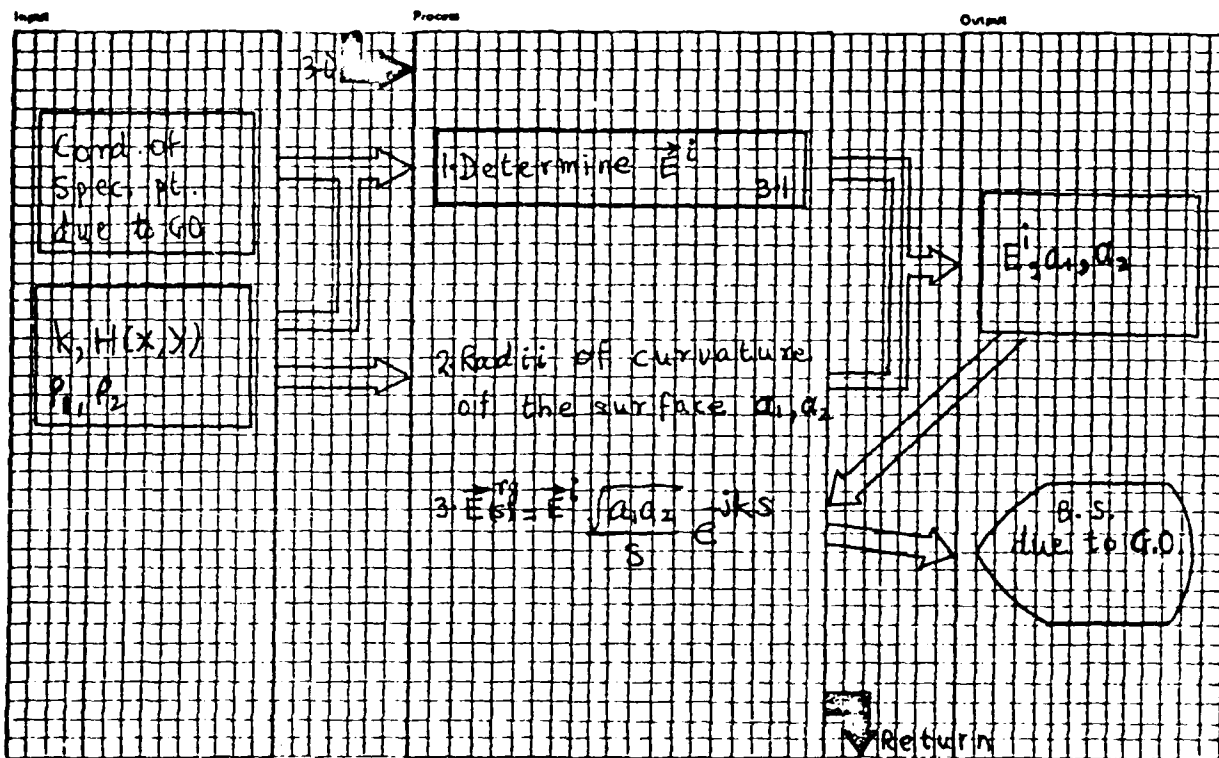
Page 726/78

7. 11/11/2023

Page 10. 3.2

Name: BSDPI

Progress B.S. at Observation pt.

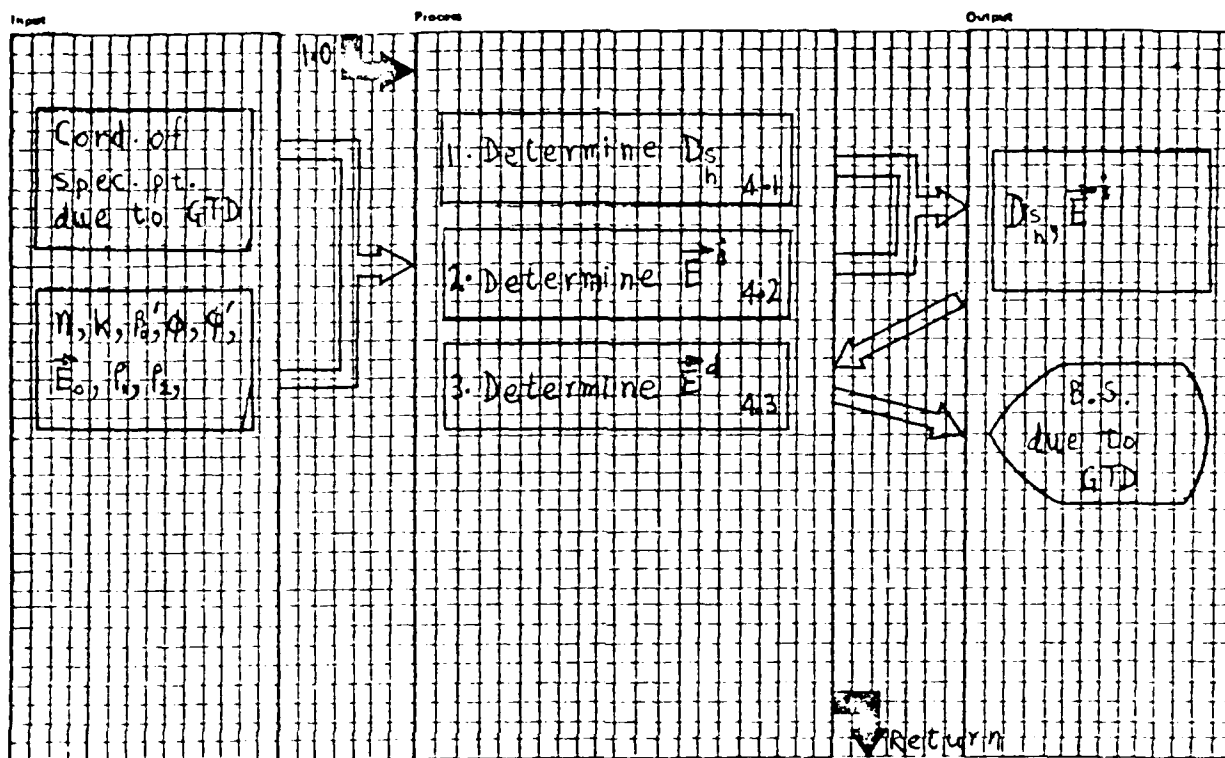
[illegible]

* The number of stores per pod may vary slightly

HIPO WORKSHEET

GX20-1970-0 U/M 025
Printed in U.S.A.

Author: A.P. Nayak System/Program: B.S. from 3-D Objects Date: 7/26/78 8 12
Diagram ID: 4.0 Name: CBSGTD Description: Calculate B.S. by GTD

[illegible]

* The number of persons per day is 74,000.

Autr. A. J. Novak

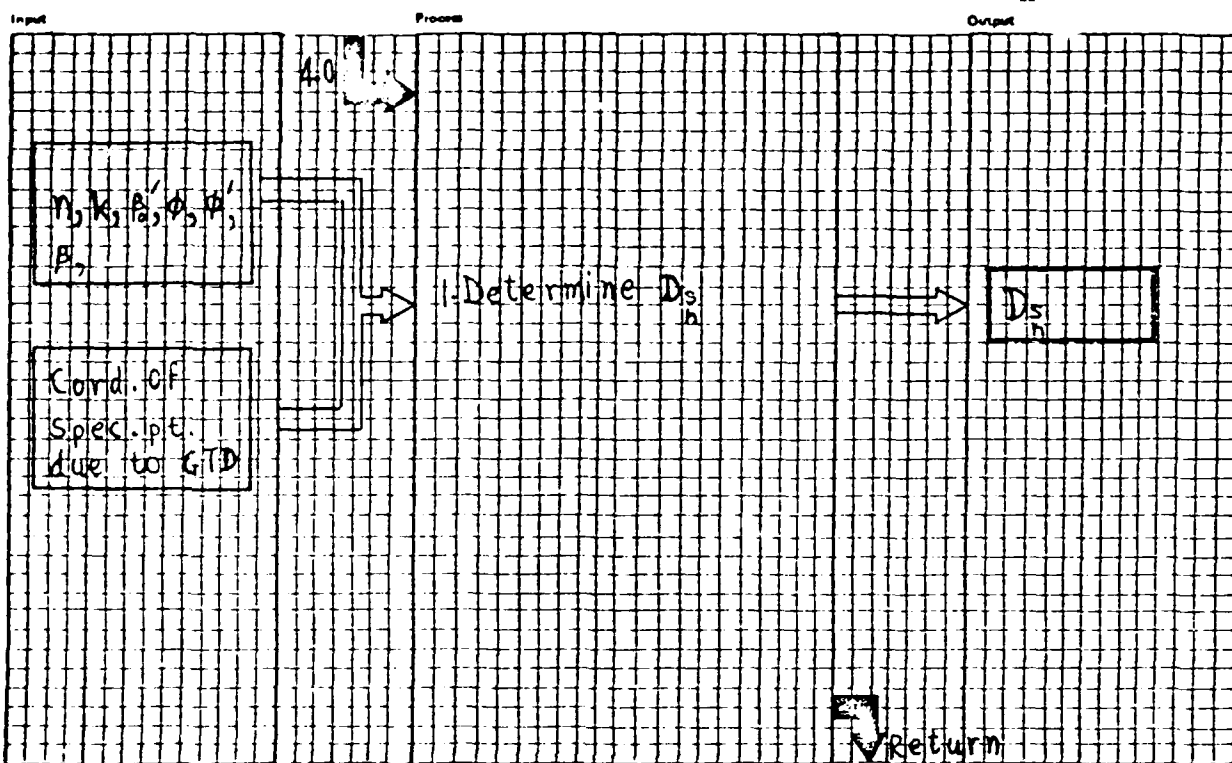
8-story Picture: B.S. from 3-D Objects

Page 7/26/78, 9 12

Doc ID: 4.1

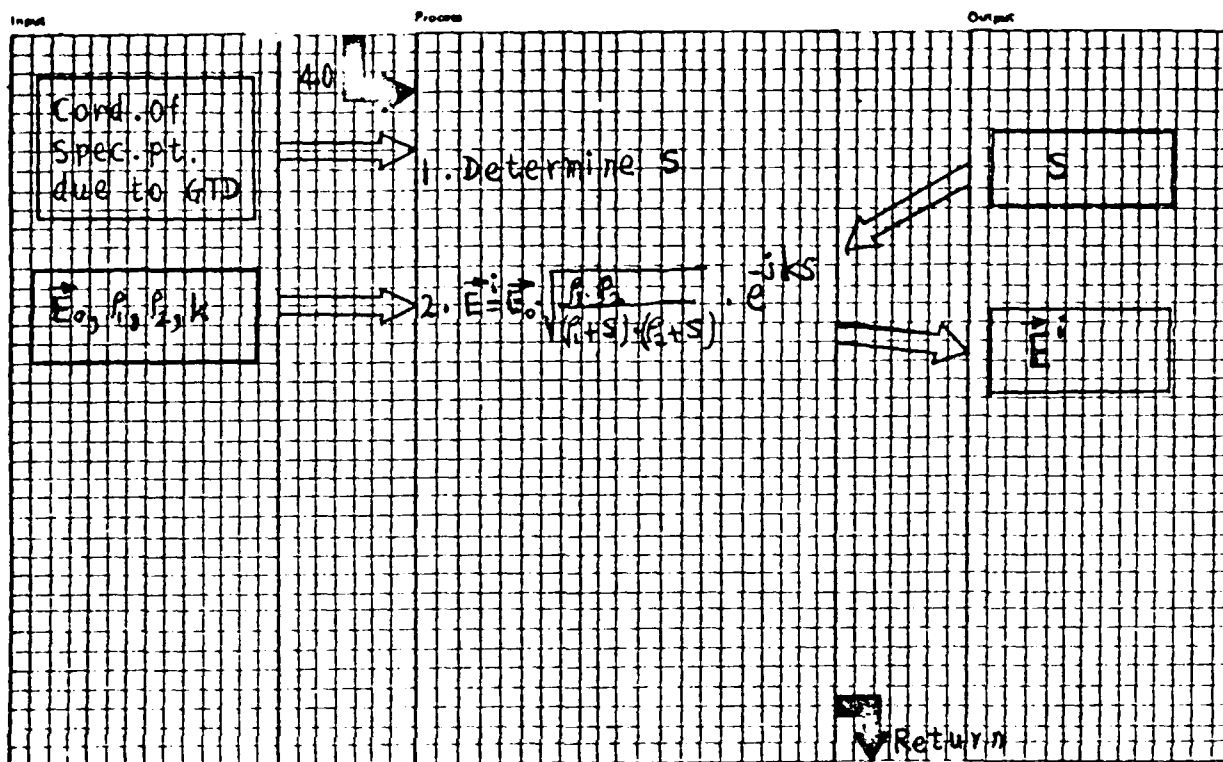
Number: CD

Description: Calculate D

[illegible]

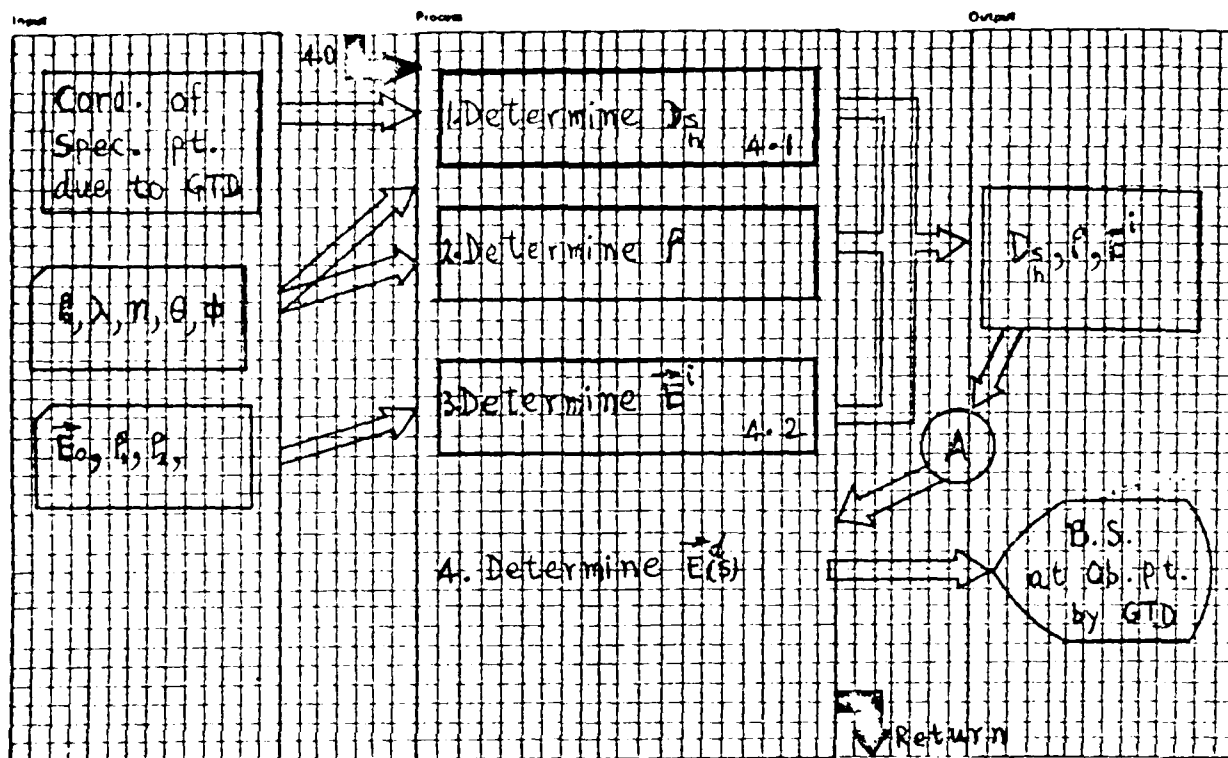
* The number of sites per pad may vary slightly

Author A. A. S. Gink System/Program B.S. from 3-D Objects Date 7/26/78 Page 0 of 12
Diagram ID D-2 Name IFSP Description Incident Field at spec.p

[illegible]

* The number of people who may vary slightly.

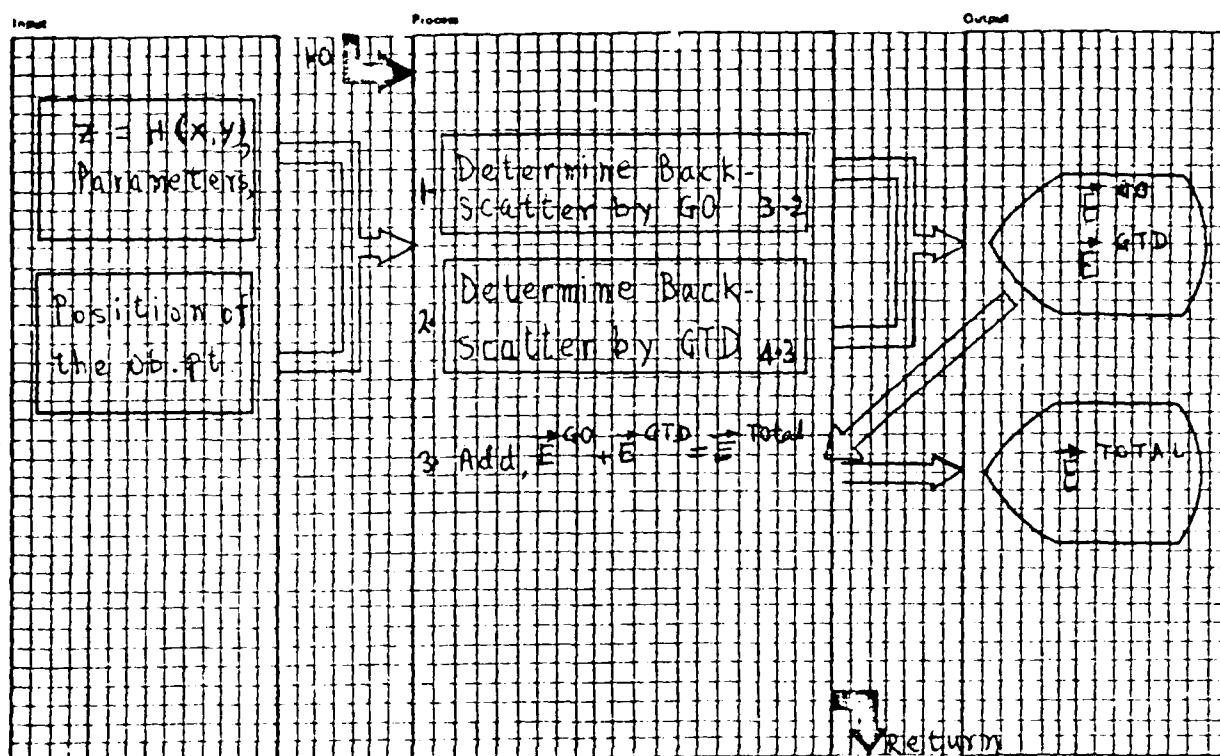
Author: A.I. York System/Program: S.Prog 3-D Objects Date: 7/26/78 Page: 11 of 12
Diagram ID: 4 Name: BSOP2 Description: S.S. at Observation pt.

[illegible]

HIPO WORKSHEET

AND USA

Author A. J. Gray System/Program 3.6.6 Rom 3-D Objects on 7/26/78 Page 12 of 12
Diagram ID 3.6 Name FEA Description Find the total field

[illegible]

END

FEB.

1988

DTic